Experimental data reduction for hyperelasticity

Marcos Latorre[a,*], Francisco J. Montáns[a]

[a]*Escuela Técnica Superior de Ingeniería Aeronáutica y del Espacio, Universidad Politécnica de Madrid, Madrid, Spain*

Abstract

WYPiWYG hyperelasticity is a data-driven, model-free computational procedure for finite element analysis of soft materials. The spline-based procedure does not assume the shape of the stored energy function and does not employ material parameters, predicting accurately any smooth prescribed behavior from a complete set of experimental tests. However, fuzzy experimental data may yield useless highly oscillatory, unstable stored energy functions, and classical curvature smoothing gives frequently unsatisfactory results. Aside, the possibility of having experimental data from different specimens for the same test was not considered in previous procedures. In this work we present a novel technique based on spline regression and smoothing penalization using stability conditions. In general, this procedure reduces noisy experimental data or data from multiple specimens for ulterior determination of the stored energy. The procedure only needs the solution of a linear system of equations. Instead of classical curvature-based smoothing, we employ a novel stability-based smoothing, determining for each branch of the uniaxial stress-strain curve the most restrictive stability condition during uniaxial and equibiaxial tests. The resulting stored energy functions are smooth and stable. The procedure has little sensitivity to the number of spline segments or to the choice of the penalization parameter, which are computed automatically.

Keywords: Hyperelasticity, WYPiWYG hyperelasticity, Soft materials, Biological tissues, Stability.

*Corresponding author

Email addresses: m.latorre.ferrus@upm.es (Marcos Latorre), fco.montans@upm.es (Francisco J. Montáns)

1. Introduction

Elastic behavior implies the absence of dissipation during any loading path. The existence of a stored elastic energy, which is the essence of hyperelasticity, guarantees the conservative behavior under elastic deformations [1], [2], [3], [4]. However, stored energy functions cannot be measured directly, so the common procedure is to propose a *model*: an analytical expression of the stored energy as a function of a strain measure. The *material parameters*, which modulate the analytical expression, are computed such that the predictions obtained from the model, for some given experiments, best-fit the available experimental data. Once determined, these material parameters may be introduced in a finite element code to predict the behavior of any structure made of that material under more general loading conditions; if the specific model is available to the user in that finite element code. The limitations of analytical expressions for stored energy functions are manifest by the number of hyperelastic models available in the literature, which according to Volokh, "is approximately equal to the number of researchers which work (or worked) in the field" [5]; some examples can be found in the reviews [6], [7], [8], [9], [10]. Then, the difficulty in selecting the appropriate model and in obtaining the corresponding material parameters is apparent and largely reported in the literature, see for example Ref. [6]. Furthermore, obtaining constitutive tangent tensors is often a difficult task [6], so numerical alternatives to avoid the tedious derivations are pursued [11], [12] even though the computational cost is obviously increased [13].

Assuming homogeneous stress and strain distributions, the typical experimental data are stress-strain pairs derived from loads and displacements. The stored energy could be obtained by integration of the corresponding partial differential equations, which constitutes the "logical chain from theory to observation" [14]. The difficulty of performing such analytical integration, in general, was remarked by Einstein in the sentence "God does not care about our mathematical difficulties; He integrates empirically" [14, p.179]; nowadays, we can integrate numerically. In this line, much attention is recently directed towards numerical data-driven, model-free constitutive modelling. One of the main reasons for addressing the problem in a way less restricted to specific assumed analytical functions is to be able to model a wider range of materials and to efficiently and accurately address patient-specific simulations [15], [16], [17]. Different approaches are currently being pursued in data-driven, model-free modelling. For example, in Ref. [18], artificial neural networks, frequently used in data-mining [19], [20], are employed to determine the constitutive behavior directly from experimental data. This procedure uses the non-affine kinematics approach of a micro-sphere model, similar to that presented by Miehe et al [21], but does not rely on an explicitly assumed stress-strain relation. Other approaches by Ibañez et al [22],

[23] are more general and seek to completely avoid making assumptions regarding the constitutive or the internal kinematic relations, and to also work directly with raw experimental data. In [22], [23], an iterative procedure is developed to obtain the intersection between the so-called constitutive manifold and the equilibrium manifold. This intersection contains the locus of the points which satisfy the weak form of the problem. These procedures have, to date, been developed at small strains. Other recent approach using small strains is given by Kirchdoerfer and Ortiz [24], [25]. In their procedure, they introduce local penalty functions to be minimized, consisting of fictitious elastic and complementary energies in which the stiffness is of numerical nature, not a material property. These functions represent an error distance of the stress-strain solution to the available material data set. In general, a drawback of all these procedures, when compared to analytical models, is that they are substantially less efficient and physical insight is lost.

What-You-Prescribe-is-What-You-Get (WYPiWYG) constitutive modeling [26], [27] is a phenomenological, purely numerical, data-driven approach to model hyperelasticity. Remarkably, the efficiency of these models under general loading is of the same order as that of analytical models [27]. The first procedure of this kind was developed by Sussman and Bathe for isotropic, incompressible materials [28]. The Sussman-Bathe procedure uses the Kearsley-Zapas inversion formula [29] to numerically obtain the stored energy function in the Valanis-Landel form [3], [30] without specifying its shape through analytical expressions. The ideas have been extended to compressible materials [27] and to anisotropic materials [31], [26], including also damage evolution [32] and viscous effects [33]. The name WYPiWYG reflects the fact that, in contrast to models based on predefined analytical functions, the procedure is capable of exactly capturing smooth experimental (or prescribed) stress-strain curves. For the isotropic case, it reproduces the results of analytical models to a high precision under any loading condition during a finite element simulation [27]. In the anisotropic case, they capture exactly as many smooth curves as independent modes in the corresponding infinitesimal theory. In contrast to many models using analytical functions, WYPiWYG hyperelasticity not only recovers the full infinitesimal theory in the limit [34] (a relevant aspect in soft materials analyzed, for example, by Murphy in Ref. [35]) but, more importantly in practice, at all deformation levels [36]. Some of the most recent advances in the WYPiWYG modeling philosophy can be found in Ref. [37].

However, one of the practical limitations of the WYPiWYG procedures is to obtain the stored energy function when fuzzy experimental information is available, which is a very frequent case, specially in soft biological tissues. Experimental curves are frequently not smooth, having relevant experimental noise. In this case, the

desired "model" curve is not the one that interpolates the experimental data, but some smoothed one. Furthermore, it is frequent that several experimental curves, from different specimens, are available for the same material. Hence, the desired "model" curve is somehow a curve that averages the complete set of experimental data points and results in a stable behavior (if that stable behavior was observed in experiments). Note that even in the case of (nonlinear) analytical models, the material parameters should not be the average of the different fits because non-physical behavior can be obtained as a result [38], [39]. The numerical procedures for WYPiWYG hyperelasticity presented in the previous works are based on piecewise cubic interpolation, with known oscillation problems even for small perturbations of the data. These oscillations may also yield unstable stored energies for materials which behave in a stable manner during the performed experimental tests. Then, a slight smoothing of experimental data was frequently necessary so that both the input (experimental) and the output (strain energy) curves had the desired smoothness. That slight smoothing was performed successfully in some works [40], [41] employing penalized splines.

Penalized splines have been used for over a decade in many fields, specially in economics, data mining and medicine, in order to obtain tendencies of observed data without unwanted oscillations [42], [43], [44], [45], [46], [47], [48], [49]. Although most publications perform smoothing with the curvature and then impose convexity or other desired conditions via lagrange multipliers [42], projections [50] or adaptive techniques [51], other alternatives have been devised in order to impose the shape or the convexity from the outset, as it is the case of exponential splines, see for example [52], [53], among others. Within the problem at hand of determining the hyperelastic stored energy of a material, smoothed splines facilitate an approach to reduce data for ulterior characterization. This data reduction is valid in general for any hyperelastic model, and it is in fact independent of it. Arguably, the problem may be less important in classical hyperelasticity using analytical functions, because the assumed "model" function with already imposed desired properties is best-fitted to whatever experimental data is available; but we note that stability constrains may also be necessary on the material constants to enforce stability. In WYPiWYG hyperelasticity the problem is more relevant, because no analytical "smooth" function is assumed: the solution is computed directly from experimental data. A background in spline interpolation may be found in Ref. [54], and in spline smoothing in Refs. [55] and [56]. An early review may be found in Ref. [57].

Therefore, the purpose of the present manuscript is to extend some of the contents advanced in [37], presenting, for the first time, a new numerical procedure specially suited for WYPiWYG hyperelasticity (although valid in general for hyperelasticity)

which is reliable for fuzzy experimental data, i.e. for data with significant experimental errors or data from different test specimens. Remarkably, it will be seen that the ordinary curvature smoothing employed in most fields in the literature is useful only for small perturbations of experimental data, and does not guarantee the stability of the resulting stored energy function. We will then introduce a penalty function based on stability conditions, suited for generic hyperelasticity, which produces excellent and robust results even for largely perturbed data. In this paper we present the ideas using the simple isotropic incompressible formulation (i.e. the Sussman-Bathe case). The anisotropic case, which is much more involved, is ongoing research.

2. A smoothing-based regression function for hyperelasticity

Consider, as an introductory (illustrative) example, the Valanis-Landel decomposition of the stored energy function for incompressible, isotropic materials, which has been verified to hold approximately for the typical strains found in polymers and biological tissues, and it is used by many analytical models [3], [30]

$$\mathcal{W}\left(E_1, E_2, E_3\right) = \omega\left(E_1\right) + \omega\left(E_2\right) + \omega\left(E_3\right) \tag{1}$$

where $E_i = \ln\left(\lambda_i\right)$ are the principal logarithmic strains, and λ_i are the principal stretches. The incompressibility condition $E_1 + E_2 + E_3 = 0$ applies. For these materials, the equilibrium equation of a uniaxial test is [28]

$$\begin{aligned} \sigma_u\left(E_u\right) &= \left.\frac{d\omega\left(E\right)}{dE}\right|_{E=E_u} - \left.\frac{d\omega\left(E\right)}{dE}\right|_{E=-\frac{1}{2}E_u} \\ &\equiv \omega'\left(E_u\right) - \omega'\left(-\tfrac{1}{2}E_u\right) \end{aligned} \tag{2}$$

where $\sigma_u\left(E_u\right)$ is the uniaxial stress-strain curve in terms of Cauchy stresses $\sigma_u \equiv \sigma_1$ and Logarithmic strains $E_u \equiv E_1$, and the second line introduces a convenient notation. The pressure-like Lagrange multiplier is determined, and substituted in Eq. (2), from equilibrium in the transverse direction employing the incompressibility condition. If both tension and compression data points (or an equivalent set of points) are known, then the Valanis-Landel function is uniquely determined within the region of interest [58]. Typically, in this simple case, a set of experimental data points $\{\hat{E}_i, \hat{\sigma}_i\}$, $i = 1, ..., N$, is intended to fit by a "model" curve $\sigma_u\left(E_u\right)$, which is controlled by a certain number of "model" unknowns numerically determined from an optimization procedure [59].

We consider herein a more general case, in which the function to be minimized is

based on the following expression

$$f\left(\boldsymbol{\sigma},\hat{\boldsymbol{\sigma}}\right)=\left(1-q\right)\hat{f}\left(\boldsymbol{\sigma},\hat{\boldsymbol{\sigma}}\right)+q\tilde{f}\left(\sigma\right) \tag{3}$$

where $\hat{\boldsymbol{\sigma}}(\hat{\boldsymbol{E}})$ is the array of the N–*experimental* stress data for the corresponding strains $\hat{\boldsymbol{E}}$ obtained from uniaxial tests. The array $\boldsymbol{\sigma}(\hat{\boldsymbol{E}})$ contains the *analytically calculated* $\sigma\left(E\right)$ stress-curve values at the given experimental strain data values $\hat{\boldsymbol{E}}$. In this paper, the hat decoration refers to experimental values, whereas the absence of it refers to analytical or computational ones. Thus $\sigma\left(E\right)$ is the assumed analytical continuous function, $\{\hat{E}_i,\hat{\sigma}_i\}$, $i=1,...,N$ are the experimental data pairs and $\{\hat{E}_i,\sigma_i\}$ are their corresponding predictions. The function $\hat{f}\left(\boldsymbol{\sigma},\hat{\boldsymbol{\sigma}}\right)$ is the (error, regression) fitting function, i.e. it contains how the discrepancy between the experimental data $\hat{\boldsymbol{\sigma}}$ and the analytical predictions $\boldsymbol{\sigma}$ is measured. The function $\tilde{f}\left(\sigma\right)$ is the smoothing function, which is usually considered only as a function of the analytical function $\sigma\left(E\right)$. The parameter q is the smoothing parameter. As given by Equation (3), the value of $q=0$ implies that no smoothing takes place, whereas values $q\to 1$ will provide strong smoothing neglecting experimental data. However, the actual effect of a particular value of q depends also on the nature of the fitting and smoothing functions.

Both the fitting and smoothing functions may be further decomposed in other functions to take into account, and weight, different possibilities. Obviously, fitting a curve in the σ-axis yields in general different results than doing so in the P-axis (or in any other stress measure). Only in some particular cases the result is the same, which are the interpolant cases, or when errors are measured in relative terms. We see next that both cases end up resulting in just different weights.

3. The regression function $\hat{f}$

We briefly describe in this section the weighted (least squares) residual $\hat{f}$. The novel finding in this work, however, concerns the smoothing function $\tilde{f}$, which is described in the next sections in detail.

3.1. Regression to experimental data in the σ-axis

The error function we use in this case accounts for the weighted difference between the available experimental data $\hat{\sigma}_i$ and the predictions σ_i resulting from the "model" curve $\sigma\left(E\right)$

$$\hat{f}_{\sigma}\left(\boldsymbol{\sigma},\hat{\boldsymbol{\sigma}};\boldsymbol{W}_{\sigma}\right)=\frac{1}{2N}\sum_{i=1}^{N}W_{\sigma i}\left(\sigma_i-\hat{\sigma}_i\right)^2=\frac{1}{2N}\left(\boldsymbol{\sigma}-\hat{\boldsymbol{\sigma}}\right)^T\boldsymbol{W}_{\sigma}\left(\boldsymbol{\sigma}-\hat{\boldsymbol{\sigma}}\right) \tag{4}$$

where $W_{\sigma i}$ are convenient weight values (typically the identity) for the N experimental data and $\boldsymbol{W}_\sigma$ is the diagonal matrix containing those values. The weight matrix may be used to assign more importance to some parts of the experimental data. We could also use it to enforce that the analytical stress-strain curve passes through the origin (if originally it does not), even in the case that experimental data does not. We would do so adding a virtual experimental pair at the origin and assigning it a large weight.

3.2. Regression to experimental data in the P-axis

Given some experimental data $\hat{\boldsymbol{\sigma}}(\hat{\boldsymbol{E}})$ in principal stress-strain directions, the experimental nominal stresses are obtained immediately by $\hat{P}_i = \exp\left(-\hat{E}_i\right)\hat{\sigma}_i$, for each $i = 1, ..., N$, and the analytical ones as $P_i = \exp\left(-\hat{E}_i\right)\sigma_i$. Hence the weighted error function is, in this case

$$\hat{f}_P\left(\boldsymbol{P}, \hat{\boldsymbol{P}}; \boldsymbol{W}_P\right) = \frac{1}{2N}\left(\boldsymbol{P} - \hat{\boldsymbol{P}}\right)^T \boldsymbol{W}_P \left(\boldsymbol{P} - \hat{\boldsymbol{P}}\right) = \frac{1}{2N}\left(\boldsymbol{\sigma} - \hat{\boldsymbol{\sigma}}\right)^T \bar{\boldsymbol{W}}_P \left(\boldsymbol{\sigma} - \hat{\boldsymbol{\sigma}}\right) \tag{5}$$

where the values of the modified diagonal matrix $\bar{\boldsymbol{W}}_P$ are

$$\bar{W}_{Pi} = W_{Pi}\exp(-2\hat{E}_i) \tag{6}$$

We note that defining

$$\boldsymbol{W} := r\boldsymbol{W}_\sigma + (1-r)\,\bar{\boldsymbol{W}}_P \tag{7}$$

where r is a combination user-prescribed parameter, we have

$$\hat{f} = r\hat{f}_\sigma\left(\boldsymbol{\sigma}, \hat{\boldsymbol{\sigma}}, \boldsymbol{W}_\sigma\right) + (1-r)\,\hat{f}_P\left(\boldsymbol{P}, \hat{\boldsymbol{P}}, \boldsymbol{W}_P\right) \tag{8}$$

Then, there is no relevant extra effort in accounting for both cases simultaneously. Furthermore, if the regression is performed in relative terms, we can write

$$\sum_{i=1}^{N}\left(\frac{P_i - \hat{P}_i}{\hat{P}_i}\right)^2 W_{Pi} = \sum_{i=1}^{N}\left(\frac{\sigma_i/\hat{\lambda}_i - \hat{\sigma}_i/\hat{\lambda}_i}{\hat{\sigma}_i/\hat{\lambda}_i}\right)^2 W_{Pi} = \sum_{i=1}^{N}\left(\frac{\sigma_i - \hat{\sigma}_i}{\hat{\sigma}_i}\right)^2 W_{Pi} \tag{9}$$

so performing the regression in the σ axis in relative terms is equivalent to doing so in the P axis. In practice this regression may also be accommodated as a particular case in which the weight matrix is modified by the experimental data as

$$W_i = W_{\sigma i}/\hat{\sigma}_i^2 \tag{10}$$

For the cases $\hat{\sigma}_i = 0$, a large W_i value is taken. Note that the value of the parameter r is in this case irrelevant. However, we note that in the interpolant case, since the error becomes zero for all experimental data, the actual value of $\boldsymbol{W}$ (and hence the type of stress under consideration) is not relevant.

4. Stability inequalities

Even though unstable stored energy functions should not be ruled out from the outset, because they could be physically correct and even desired for analyzing localization phenomena [60], in usual cases, stability is a desired property, specially if that stable behavior was observed during the tests. In the examples below, we will pursue some stability conditions. In fact, these conditions will prove to be excellent penalty functions in the smoothing procedure. In this section we address some stability conditions that we can easily use in our procedure, deriving finally a unified criterion for both (tension-compression) uniaxial and equibiaxial tests. For further background on stability conditions, see for example Refs. [60], [61], [62].

4.1. Uniaxial test inequality

Using $E_u = \ln \lambda_u$ for a *uniaxial* tension-compression test, since the nominal stresses are $P_u := \sigma_u / \lambda_u$, we obtain the following relation from Eq. (2)

$$P_u(E_u) = \frac{1}{\exp(E_u)} \left[\omega'(E_u) - \omega'\left(-\tfrac{1}{2}E_u\right) \right] \tag{11}$$

where, recall, $\omega'(E_u)$ is the derivative of ω respect to E evaluated at E_u. The stability condition we will use below states that nominal stresses should increase (equivalently, decrease) with stretch during the tensile (compression) test, i.e. $S_u(E_u) := dP_u(\lambda_u)/d\lambda_u > 0$

$$S_u(E_u) = \exp(-2E_u)\, C_u(E_u) > 0 \tag{12}$$

where $\exp(-2E_u) > 0$ and we define $C_u(E_u)$ as

$$C_u(E_u) := \sigma_u'(E_u) - \sigma_u(E_u) > 0 \tag{13}$$

In terms of the stored energy function

$$C_u(E_u) = \left[\omega''(E_u) + \tfrac{1}{2}\omega''\left(-\tfrac{1}{2}E_u\right) \right] - \left[\omega'(E_u) - \omega'\left(-\tfrac{1}{2}E_u\right) \right] > 0 \tag{14}$$

which includes explicit evaluations of ω' and ω'' within both tension and compression branches [58].

4.2. Equibiaxial test inequality

Following the same procedure as before, a similar stability condition may be obtained for an equibiaxial test. If $E_e = E_2 = E_1 = \ln \lambda_1 = \ln \lambda_e$ are the logarithmic strains of the *equibiaxial* tension-compression test performed in directions 1 and 2, the nominal stresses are

$$P_e \equiv P_1 = P_2 = \frac{1}{\lambda_e}\omega'(E_e) + \frac{p}{\lambda_e} \tag{15}$$

where p is the pressure-like Lagrange multiplier associated with the incompressibility constraint. Assuming a plane stress condition and using $-2E_e = E_3 = \ln \lambda_3 = \ln \lambda_e^{-2}$ for the third axis

$$P_3 = \lambda_e^2 \omega'(-2E_e) + \lambda_e^2 p = 0 \tag{16}$$

from which the pressure-like unknown is factored-out as $p = -\omega'(-2E_e)$. Then, the equibiaxial nominal stress is

$$P_e(E_e) = \frac{1}{\exp(E_e)}\left[\omega'(E_e) - \omega'(-2E_e)\right] \tag{17}$$

The Cauchy stresses are

$$\sigma_e(E_e) = \exp(E_e) P_e(E_e) = \omega'(E_e) - \omega'(-2E_e) \tag{18}$$

The stability requirement for the equibiaxial test $S_e(E_e) := dP_e/d\lambda_e > 0$ reads

$$S_e(E_e) = \exp(-2E_e) C_e(E_e) > 0 \tag{19}$$

whereupon

$$C_e(E_e) := \sigma_e'(E_e) - \sigma_e(E_e) > 0 \tag{20}$$

and in terms of stored energy function derivatives

$$C_e(E_e) = \left[\omega''(E_e) + 2\omega''(-2E_e)\right] - \left[\omega'(E_e) - \omega'(-2E_e)\right] > 0 \tag{21}$$

Consider $\sigma_u(E_u)$ as the uniaxial stress-strain curve and $\sigma_e(E_e)$ as the equibiaxial stress-strain curve. Since the material is the same, and hence the stored energy function is also the same in both cases, the curves of both tests may be related for

a given strain value E_* by

$$\left.\begin{array}{l} \sigma_u\left(E_*\right)=\omega'\left(E_*\right)-\omega'\left(-\frac{1}{2}E_*\right) \\ \sigma_e\left(E_*\right)=\omega'\left(E_*\right)-\omega'\left(-2E_*\right) \end{array}\right\} \Rightarrow \left\{\begin{array}{l} \sigma_u\left(E_*\right)=-\sigma_e\left(-\frac{1}{2}E_*\right) \\ \sigma_e\left(E_*\right)=-\sigma_u\left(-2E_*\right) \end{array}\right. \tag{22}$$

and

$$\left.\begin{array}{l} \sigma_u'\left(E_*\right)=\omega''\left(E_*\right)+\frac{1}{2}\omega''\left(-\frac{1}{2}E_*\right) \\ \sigma_e'\left(E_*\right)=\omega''\left(E_*\right)+2\omega''\left(-2E_*\right) \end{array}\right\} \Longrightarrow \left\{\begin{array}{l} \sigma_u'\left(E_*\right)=\frac{1}{2}\sigma_e'\left(-\frac{1}{2}E_*\right) \\ \sigma_e'\left(E_*\right)=2\sigma_u'\left(-2E_*\right) \end{array}\right. \tag{23}$$

Therefore, Equation (20) may be written in terms of the associated uniaxial stress-strain curve data as

$$\tfrac{1}{2}C_e\left(E_e\right)=\sigma_u'\left(-2E_e\right)+\tfrac{1}{2}\sigma_u\left(-2E_e\right)>0 \tag{24}$$

where the factor $1/2$ is introduced for further convenience. Importantly, note that, for example, Eq. (24) for $E_e>0$ is evaluated at the strain $-2E_e<0$ of the equivalent uniaxial test, but it corresponds to the stability condition of the equibiaxial test at strain $E_e>0$.

4.3. Unified tension/compression uniaxial/equibiaxial inequality

We say that Eq. (13) is a *direct* stability condition for the uniaxial test curve because it has been derived *directly* from the uniaxial test. As we have just seen, Eq. (24) imposes an additional restriction for the uniaxial test curve in terms of the associated equibiaxial response. We say that Eq. (24) is an *indirect* stability condition for the uniaxial test curve because it has been derived *indirectly* from the equibiaxial test. Therefore, we have two different mathematical stability conditions for each branch of the uniaxial test, which obviously refer to two different physical requirements. We will consider the more restrictive condition for each part of the domain in the stability analysis of the material at hand, meaning that we require the material to be stable during both tension-compression uniaxial and equibiaxial tests.

Consider an arbitrary (compression) uniaxial state such that $E_*=\ln\lambda_*<0$. If we require $dP_u/d\lambda_u>0$ for all $\lambda_*<1$ and, as usual, $P_u(\lambda_u=1)=0$, then $P_u\left(\lambda_*\right)<0$

and $\sigma_u(E_*) = \lambda_* P_u(\lambda_*) < 0$ as well. Then

$$\begin{aligned} C_u(E_*) &= \sigma_u'(E_*) - \sigma_u(E_*) \\ &> \sigma_u'(E_*) + \tfrac{1}{2}\sigma_u(E_*) = \tfrac{1}{2} C_e\left(-\tfrac{1}{2}E_*\right) > 0 \end{aligned} \tag{25}$$

i.e. the requirement $\frac{1}{2}C_e\left(-\frac{1}{2}E_*\right) > 0$ is more restrictive than $C_u(E_*) > 0$ when $E_* < 0$. We can express this result as—note that the factor $1/2$ is irrelevant here

$$C_e\left(-\tfrac{1}{2}E_*\right) > 0 \quad \Rightarrow \quad C_u(E_*) > 0\,, \quad \text{for } E_* < 0 \tag{26}$$

or, in terms of the nominal stresses in the respective tests, as

$$\begin{aligned} &\left.\frac{dP_e}{d\lambda_e}\right|_{\lambda_e} > 0 \quad \Rightarrow \quad \left.\frac{dP_u}{d\lambda_u}\right|_{\lambda_u} > 0 \\ &\text{for } \lambda_e = \frac{1}{\lambda_u^{1/2}} > 1 \text{ and } \lambda_u < 1 \end{aligned} \tag{27}$$

Note that the reciprocal statements are not satisfied, in general.

Proceeding in the same way, we can also compare the conditions $dP_u/d\lambda_u > 0$ for $\lambda_u > 1$ and $dP_e/d\lambda_e > 0$ for $\lambda_e = 1/\lambda_u^{1/2} < 1$, both expressed in terms of uniaxial relations, in order to see what condition is more restrictive in the equivalent tension-uniaxial / compression-equibiaxial states. The *direct* and *indirect* uniaxial stability conditions are given in Eqs. (13) and (24), which in this case are to be analyzed for an arbitrary strain value $E_* > 0$, yielding

$$\tfrac{1}{2}C_e\left(-\tfrac{1}{2}E_*\right) = \sigma_u'(E_*) + \tfrac{1}{2}\sigma_u(E_*) > \sigma_u'(E_*) - \sigma_u(E_*) = C_u(E_*) > 0 \tag{28}$$

where we have used the fact that $\sigma_u(E_*) = \lambda_* P_u(\lambda_*) > 0$ during the tensile test. Thus, in this case the uniaxial condition $C_u(E_*) > 0$ assess the stable response during the compression equibiaxial test, i.e.

$$C_u(E_*) > 0 \quad \Rightarrow \quad C_e\left(-\tfrac{1}{2}E_*\right) > 0\,, \quad \text{for } E_* > 0 \tag{29}$$

or

$$\begin{aligned} &\left.\frac{dP_u}{d\lambda_u}\right|_{\lambda_u} > 0 \quad \Rightarrow \quad \left.\frac{dP_e}{d\lambda_e}\right|_{\lambda_e} > 0 \\ &\text{for } \lambda_u > 1 \text{ and } \lambda_e = \frac{1}{\lambda_u^{1/2}} < 1 \end{aligned} \tag{30}$$

Hence, the stability criteria

$$C(E) = \begin{cases} \sigma_u'(E) - \sigma_u(E) > 0 & , \quad \text{for } E > 0 \\ 2\sigma_u'(E) + \sigma_u(E) > 0 & , \quad \text{for } E < 0 \end{cases} \tag{31}$$

guarantee that all the responses, both under tension and compression, are stable in the sense that $dP/d\lambda > 0$ for both the uniaxial and the equibiaxial tests, and will be the ones we consider.

5. A stability-based smoothing function $\tilde{f}$

When data dispersion is large, the stored energy function obtained from usual regression procedures may result in unstable behavior, even when the material was behaving in a stable manner during the tests. Therefore, we want to guarantee some stability constraints. These stability constraints may be imposed either strictly, for example through Lagrange multipliers, or through penalty functions. The strict imposition of the equations, point by point, result in a nonlinear system of equations and, usually, uniqueness of solution (and a global minimum) cannot be guaranteed. We have performed numerical experiments using these possibilities and despite of the increased numerical effort, the results have been in general rather disappointing and not robust. Hence we follow here a different approach which has proven successful not only in guaranteeing stability, but also in properly smoothing the stress-strain data and, hence, the corresponding stored energy function.

The procedure we present in this section is to impose the constraints via penalty procedures under the assumption that the material is overall stable in the strain domain, that is, a physically-oriented smoothing based on stability considerations. We will take as constraints the stability during the uniaxial tension test and the stability during the equibiaxial tension test, which guarantee the stability in terms of nominal stresses for both tension and compression behaviors during both types of tests, as we showed above. We assess these criteria using the experimental curve from a uniaxial test, including the compression branch obtained either from compression or from equibiaxial tests. Similar procedures may be developed for other conditions following the same guidelines.

The constraint condition for the uniaxial test under tension, Eq. $(31)_1$, may be written as

$$C^+\left(\bar{E}^+\right) := C_u\left(\bar{E}^+\right) = \sigma_u'\left(\bar{E}^+\right) - \sigma_u\left(\bar{E}^+\right) \tag{32}$$

where $\bar{E}_i^+ > 0$ are the strain values at which the constraint is evaluated. For the uniaxial compression branch, we enforce the stability indirectly through the tension

equibiaxial test, i.e. in terms of uniaxial stress-strain curves, see Eq. $(31)_2$

$$C^{-}\left(\bar{E}^{-}\right) := C_e\left(-\tfrac{1}{2}\bar{E}^{-}\right) = 2\sigma_u'\left(\bar{E}^{-}\right) + \sigma_u\left(\bar{E}^{-}\right) \tag{33}$$

where $\bar{E}_i^{-} < 0$. The basic idea for generating the penalty function is to assume that the material is overall stable so in the domain of interest we mostly have $C\left(E\right) > 0$. The penalty function penalizes large variations in the stability function $S\left(E\right)$, so local unstabilities will be prevented. For the tension branch $E \geq 0$, Eq. (12), we define $S^{+}\left(E \geq 0\right)$ as

$$S^{+}\left(E\right) := S_u\left(E\right) = \left.\frac{dP_u\left(\lambda_u\right)}{d\lambda_u}\right|_{\lambda_u = \exp(E)} = \exp\left(-2E\right) C^{+}\left(E\right) \ , \quad \text{with } E \geq 0 \tag{34}$$

so

$$\frac{dS^{+}\left(E\right)}{dE} = \exp\left(-2E\right)\left[-2C^{+}\left(E\right) + \frac{dC^{+}\left(E\right)}{dE}\right] \tag{35}$$

In a similar way, for the compression branch $E < 0$, Eq. (19), we define $S^{-}\left(E < 0\right)$ as—note that we have already defined $C^{-}\left(E < 0\right)$ in Eq. (33) based on $(31)_2$

$$S^{-}\left(E\right) := S_e\left(-\tfrac{1}{2}E\right) = \left.\frac{dP_e\left(\lambda_e\right)}{d\lambda_e}\right|_{\lambda_e = \exp(-\frac{1}{2}E)} = \exp\left(E\right) C^{-}\left(E\right) \ , \quad \text{with } E < 0 \tag{36}$$

so

$$\frac{dS^{-}\left(E\right)}{dE} = \exp\left(E\right)\left[C^{-}\left(E\right) + \frac{dC^{-}\left(E\right)}{dE}\right] \tag{37}$$

Then we can define a stability smoothing "function" $\tilde{f}$, to be used in Eq. (3), as

$$\tilde{f} = \frac{\displaystyle\int_{E_{\min}}^{0}\left(\frac{dS^{-}\left(E\right)}{dE}\right)^2 dE + \int_{0}^{E_{\max}}\left(\frac{dS^{+}\left(E\right)}{dE}\right)^2 dE}{\displaystyle\int_{E_{\min}}^{E_{\max}} dE} \tag{38}$$

6. A curvature-based smoothing function $\tilde{f}$

Another smoothing condition that we could use as $\tilde{f}$ in Eq. (3) is based on the curvature of the stress-strain curve considered. We will see in the examples below, however, that this smoothing technique, employed in many fields in the literature, is useful only when data dispersion is small. The translation of the usual smoothing

employed in the literature to hyperelasticity consists of performing a smoothing based on the second derivative of either the $\sigma(E)$ curve or the $P(\lambda)$ curve. Then, we can take either the following smoothing "function"

$$\tilde{f}_{\sigma} = \frac{\displaystyle\int_{E_{\min}}^{E_{\max}} (\sigma'')^2 \, dE}{\displaystyle\int_{E_{\min}}^{E_{\max}} dE} \tag{39}$$

or, considering the $P - \lambda$ axes,

$$\tilde{f}_{P} = \frac{\displaystyle\int_{\lambda_{\min}}^{\lambda_{\max}} \left(P_j''(\lambda)\right)^2 \, d\lambda}{\displaystyle\int_{\lambda_{\min}}^{\lambda_{\max}} d\lambda} \tag{40}$$

We note that, similarly to Eq. (8), both smoothings can be combined as

$$\tilde{f} \equiv s\tilde{f}_{\sigma} + (1-s)\,\tilde{f}_{P} \tag{41}$$

where s is a combination parameter.

Hence, in this work, we are substituting this geometrically-oriented smoothing (based on curvature) by a physically-oriented smoothing (based on stability).

7. Smoothing regression splines for hyperelasticity

The procedure we presented above can be applied to any strain energy function expressed in Valanis–Landel form. In addition, we note that stability conditions on $\mathcal{W}$ can be imposed directly to the stored energy function terms $\omega(E)$ or to the tensile test curve. We use in this section WYPiWYG hyperelasticity and consider the curve fitting procedure entirely on the uniaxial stress-strain curve, addressing directly the stability constraints on the stress-strain curve during the fitting procedure.

7.1. Regression to experimental data

The stress function $\boldsymbol{\sigma}(\hat{\boldsymbol{E}})$, for the case in which the B-spline parameter is chosen to be $t \equiv x \equiv E$, is given as a function of the $n-$vertices $\boldsymbol{B}$ of the control polygon as —see Appendix

$$\boldsymbol{\sigma}(\hat{\boldsymbol{E}}) = \hat{\boldsymbol{N}}\boldsymbol{B} \tag{42}$$

where we defined for clarity of notation $\hat{\boldsymbol{N}} = \boldsymbol{N}(\hat{\boldsymbol{E}})$. The error term of the objective function, Eq. (4), reads

$$\hat{f}_\sigma\left(\boldsymbol{\sigma}, \hat{\boldsymbol{\sigma}}; \boldsymbol{W}_\sigma\right) = \frac{1}{2N}\boldsymbol{B}^T\hat{\boldsymbol{N}}^T\boldsymbol{W}_\sigma\hat{\boldsymbol{N}}\boldsymbol{B} - \frac{1}{N}\hat{\boldsymbol{\sigma}}^T\boldsymbol{W}_\sigma\hat{\boldsymbol{N}}\boldsymbol{B} + const \tag{43}$$

where the constant term is irrelevant for our purposes.

The weighted error function, Eq. (5), is in this case

$$\hat{f}_P\left(\boldsymbol{P}, \hat{\boldsymbol{P}}; \boldsymbol{W}_P\right) = \frac{1}{2N}\boldsymbol{B}^T\hat{\boldsymbol{N}}^T\bar{\boldsymbol{W}}_P\hat{\boldsymbol{N}}\boldsymbol{B} - \frac{1}{N}\hat{\boldsymbol{\sigma}}^T\bar{\boldsymbol{W}}_P\hat{\boldsymbol{N}}\boldsymbol{B} + const \tag{44}$$

7.2. Curvature-based smoothing

We use a normalized parameter ξ to systematically describe each spline polynomial defined between two given strain values using the same general expression. This normalized parameter, within the interval $E \in [E_j, E_{j+1}]$, is

$$\xi = \frac{E - E_j}{E_{j+1} - E_j} \tag{45}$$

so

$$\frac{d\xi}{dE} = \frac{1}{\Delta E_j} \text{ and } d^2\xi/dE^2 = 0 \tag{46}$$

with $\Delta E_j := E_{j+1} - E_j$. Recall that we take for periodic splines the parametrization $E \equiv t$, see Appendix. Derivatives of periodic normalized B-splines (and also of the corresponding piecewise cubic splines) are given by immediate derivation of Eq. (82) as in Eq. (84) of the appendix. Then, for the case in which we use $\sigma''(E)$, taking the stresses in the $j-$piece as $\sigma_j(E) = \mathfrak{P}_j(\xi(E))$, where $\mathfrak{P}_j$ is the corresponding polynomial (see Appendix) we have

$$\begin{aligned}\int_{E_{\min}}^{E_{\max}} \left(\sigma_j''(E)\right)^2 dE &= \sum_{j=1}^{m} \int_{E_j}^{E_{j+1}} \left(\sigma_j''\right)^2 dE \\ &= \sum_{j=1}^{m} \boldsymbol{B}_j^T\bar{\boldsymbol{N}}^T\boldsymbol{A}_E\bar{\boldsymbol{N}}\boldsymbol{B}_j = \boldsymbol{B}^T\boldsymbol{\Lambda}_E\boldsymbol{B}\end{aligned} \tag{47}$$

where the prima accent indicates derivative respect to the argument in parenthesis and we defined

$$\boldsymbol{A}_E := \frac{1}{\Delta E_j^3}\left[\int_0^1 \left(\boldsymbol{\Xi}''\right)^T \left(\boldsymbol{\Xi}''\right) d\bar{\xi}\right] = \frac{1}{\Delta E_j^3}\begin{bmatrix} 12 & 6 & 0 & 0 \\ 6 & 4 & 0 & 0 \\ 0 & 0 & 0 & 0 \\ 0 & 0 & 0 & 0 \end{bmatrix} \tag{48}$$

and m is the number of segments, see Figure 10 in the appendix. The last identity in Eq. (47) is obtained through the assembly of the addends in a similar way as in the finite elements context:

$$\boldsymbol{\Lambda}_E = \bigwedge_{j=1}^{m} \bar{\boldsymbol{N}}^T \boldsymbol{A}_E \bar{\boldsymbol{N}} \text{ and } \boldsymbol{B} = \bigwedge_{j=1}^{m} \boldsymbol{B}_j \tag{49}$$

The assembly operator, denoted by $\wedge$, is performed using equal matrices if ΔE_j is constant, so the procedure is computationally very efficient. On the other hand, for the case of equal intervals, $E_{\max} - E_{\min} = m\Delta E$, so Eq. (39) finally reads

$$\tilde{f}_\sigma = \frac{1}{m\Delta E}\boldsymbol{B}^T \boldsymbol{\Lambda}_E \boldsymbol{B} \tag{50}$$

Regarding the smoothing in the $P-\lambda$ axes, the logarithmic strains $E = \ln\lambda$ give the relation

$$\xi = \frac{\ln\lambda - E_j}{E_{j+1} - E_j} \quad \text{and} \quad \lambda = \exp\left(\Delta E_j \xi + E_j\right) \tag{51}$$

and $d\lambda = \lambda \Delta E_j d\xi$. Using Eqs. (82) and (84) of the appendix, after some algebra we can write

$$\sum_{j=1}^{m} \int_{\lambda_j}^{\lambda_{j+1}} \left(P_j''(\lambda)\right)^2 d\lambda = \sum_{j=1}^{m} \boldsymbol{B}_j^T \bar{\boldsymbol{N}}^T \boldsymbol{A}_{Pj} \bar{\boldsymbol{N}} \boldsymbol{B}_j = \boldsymbol{B}^T \boldsymbol{\Lambda}_\lambda \boldsymbol{B} \tag{52}$$

where

$$\boldsymbol{A}_{Pj} := \frac{1}{\Delta E_j^3 \exp\left(5E_j\right)} \int_0^1 \frac{1}{\exp\left(5\Delta E_j \xi\right)} \left[\boldsymbol{\Xi}^*(\xi)\right]^T \boldsymbol{\Xi}^*(\xi)\, d\xi \tag{53}$$

and

$$\boldsymbol{\Xi}^*(\xi) := 2\Delta E_j^2 \boldsymbol{\Xi}(\xi) - 3\Delta E_j \boldsymbol{\Xi}'(\xi) + \boldsymbol{\Xi}''(\xi) \tag{54}$$

and

$$\boldsymbol{\Lambda}_\lambda = \bigwedge_{j=1}^{m} \bar{\boldsymbol{N}}^T \boldsymbol{A}_{Pj} \bar{\boldsymbol{N}} \tag{55}$$

Taking into account that $\lambda_{\max} - \lambda_{\min} =: \delta\lambda$, Eq. (40) yields

$$\tilde{f}_P = \frac{1}{\delta\lambda} \boldsymbol{B}^T \boldsymbol{\Lambda}_\lambda \boldsymbol{B} \tag{56}$$

The combined expression Eq. (41) is then $\tilde{f} = \frac{1}{2} q \boldsymbol{B}^T \boldsymbol{\Lambda} \boldsymbol{B}$ where

$$\boldsymbol{\Lambda} := \frac{s}{\delta E} \boldsymbol{\Lambda}_E + \frac{(1-s)}{\delta\lambda} \boldsymbol{\Lambda}_\lambda \tag{57}$$

This expression reveals that smoothing in either $\sigma - E$ or $P - \lambda$ is simply taken into account through different $\boldsymbol{\Lambda}$ operators.

7.3. Stability-based smoothing

Equations (32) and (33) specialize to

$$C^+\left(\bar{E}^+\right) = \left[\boldsymbol{N}'\left(\bar{E}^+\right) - \boldsymbol{N}\left(\bar{E}^+\right)\right] \boldsymbol{B} > \boldsymbol{0} \tag{58}$$

and

$$C^-\left(\bar{E}^-\right) = \left[2\boldsymbol{N}'\left(\bar{E}^-\right) + \boldsymbol{N}\left(\bar{E}^-\right)\right] \boldsymbol{B} > \boldsymbol{0} \tag{59}$$

while Eq. (35) reads

$$\frac{dS^+(E)}{dE} = \frac{\exp(-2E)}{\Delta E^2} \boldsymbol{\Xi}_S^+ \bar{\boldsymbol{N}} \boldsymbol{B}_j \tag{60}$$

where we have used

$$\frac{dC^+}{dE^+} = \left[\boldsymbol{\Xi}''\left(\xi\left(E^+\right)\right)\left(\frac{d\xi}{dE}\right)^2 - \boldsymbol{\Xi}'\left(\xi\left(E^+\right)\right)\left(\frac{d\xi}{dE}\right)\right] \bar{\boldsymbol{N}} \boldsymbol{B}_j \tag{61}$$

with $d\xi/dE = 1/\Delta E$, and

$$\boldsymbol{\Xi}_S^+ := \boldsymbol{\Xi}'' - 3\boldsymbol{\Xi}'\Delta E + 2\boldsymbol{\Xi}\Delta E^2 \tag{62}$$

In a similar way, Eq. (37) particularizes to

$$\frac{dS^-(E)}{dE} = \frac{\exp(E)}{\Delta E^2} \boldsymbol{\Xi}_S^- \bar{\boldsymbol{N}} \boldsymbol{B}_j \tag{63}$$

with

$$\boldsymbol{\Xi}_S^- := 2\boldsymbol{\Xi}'' + 3\boldsymbol{\Xi}'\Delta E + \boldsymbol{\Xi}\Delta E^2 \tag{64}$$

Then, the integrals in Eq. (38) are evaluated through

$$\int_{E_j}^{E_{j+1}} \left(\frac{dS^+}{dE}\right)^2 dE = \boldsymbol{B}_j^T \bar{\boldsymbol{N}}^T \boldsymbol{A}_{Sj}^+ \bar{\boldsymbol{N}} \boldsymbol{B}_j \tag{65}$$

and

$$\int_{E_j}^{E_{j+1}} \left(\frac{dS^-}{dE}\right)^2 dE = \boldsymbol{B}_j^T \bar{\boldsymbol{N}}^T \boldsymbol{A}_{Sj}^- \bar{\boldsymbol{N}} \boldsymbol{B}_j \tag{66}$$

with

$$\boldsymbol{A}_{Sj}^+ = \frac{\exp\left(-4E_j\right)}{\Delta E^3} \int_0^1 \exp\left(-4\Delta E\xi\right) \boldsymbol{\Xi}_S^{+T} \boldsymbol{\Xi}_S^+ d\xi \tag{67}$$

and

$$\boldsymbol{A}_{Sj}^- = \frac{\exp\left(2E_j\right)}{\Delta E^3} \int_0^1 \exp\left(2\Delta E\xi\right) \boldsymbol{\Xi}_S^{-T} \boldsymbol{\Xi}_S^- d\xi \tag{68}$$

Finally, as before

$$\boldsymbol{\Lambda} = \boldsymbol{\Lambda}_S = \frac{1}{m\Delta E} \left(\bigwedge_{i=1}^{m^-} \bar{\boldsymbol{N}}^T \boldsymbol{A}_{Si}^- \bar{\boldsymbol{N}} + \bigwedge_{i=1}^{m^+} \bar{\boldsymbol{N}}^T \boldsymbol{A}_{Si}^+ \bar{\boldsymbol{N}} \right) \tag{69}$$

which can also be combined, if desired, with the previous smoothing functions. In summary, all smoothing possibilities may be considered with a simple change in the corresponding $\boldsymbol{\Lambda}$ matrix. Furthermore, additional weight functions could be easily accommodated without relevant changes.

7.4. Linear system of equations

The procedure described in this section results in the quadratic minimization problem

$$\begin{aligned} f\left(\boldsymbol{\sigma}\right) &= \frac{1}{2}\frac{\left(1-q\right)}{N} \boldsymbol{B}^T \hat{\boldsymbol{N}}^T \boldsymbol{W} \hat{\boldsymbol{N}} \boldsymbol{B} - \frac{\left(1-q\right)}{N} \hat{\boldsymbol{\sigma}}^T \boldsymbol{W} \hat{\boldsymbol{N}} \boldsymbol{B} + \frac{1}{2} q \boldsymbol{B}^T \boldsymbol{\Lambda} \boldsymbol{B} \\ &= \frac{1}{2} \boldsymbol{B}^T \boldsymbol{A} \boldsymbol{B} - \boldsymbol{b}^T \boldsymbol{B} \end{aligned} \tag{70}$$

where we defined

$$\boldsymbol{A} := \left[\frac{\left(1-q\right)}{N} \hat{\boldsymbol{N}}^T \boldsymbol{W} \hat{\boldsymbol{N}} + q\boldsymbol{\Lambda}\right] \quad \text{and} \quad \boldsymbol{b} := \frac{\left(1-q\right)}{N} \hat{\boldsymbol{N}}^T \boldsymbol{W} \hat{\boldsymbol{\sigma}} \tag{71}$$

whose solution for $\boldsymbol{B}$ is immediately obtained solving the following banded linear system of equations

$$\boldsymbol{A}\boldsymbol{B} = \boldsymbol{b} \tag{72}$$

Automatic smoothing may be easily obtained if we set q to be the minimum value such that $C(E) > tol > 0$ in all the domain.

8. Examples

In this section we show some examples of the performance of smoothing periodic B-splines in fitting experimental data and in obtaining stable energies. In the examples, we will use four sets of "experimental" data generated from Ogden's model

$$\mathcal{W}(\lambda_1, \lambda_2, \lambda_3) = \sum_{i=1}^{3} \mu \frac{\mu_i}{\alpha_i} \left(\lambda_1^{\alpha_i} + \lambda_2^{\alpha_i} + \lambda_3^{\alpha_i} - 3\right) \tag{73}$$

These data are shown in Figure 1. The set in Figure 1a is the prediction for Ogden's model with the parameters

$$\alpha_1 = 1.3,\ \alpha_2 = 5,\ \alpha_3 = -2 \tag{74}$$

and

$$\mu = 0.42\,\mathrm{MPa}\,,\ \mu_1 = 1.4,\ \mu_2 = 3.0 \times 10^{-3},\ \mu_3 = -24 \times 10^{-3} \tag{75}$$

so using the incompressibility condition, the $P - \lambda$ relation is

$$P(\lambda) = \mu \sum_{i=1}^{3} \mu_i \left[\lambda^{(\alpha_i - 1)} - \lambda^{\left(-\frac{1}{2}\alpha_i - 1\right)}\right] \tag{76}$$

In this case, sampling data are equispaced in the logarithmic strain space and consist of 31 stress-strain pairs. Figure 1b shows data from the same model but generated with a small random perturbation, a perturbation which is different for each computed "experimental" point. In this case, and in the following cases, sampling data are not equispaced, but generated with an additional small random perturbation also for logarithmic strains. Figure 1c shows three curves with a perturbation in μ_i and slightly different α_i exponents for each curve. Figure 1d has three curves similar to case 1c, but an additional curve in which white noise has been added.

In Figure 2 we show the predictions for experimental data in Figure 1a using 31 vertices, the same number as actual experimental data so B-splines become interpolant. In all cases in this paper, to guarantee that predictions pass through the

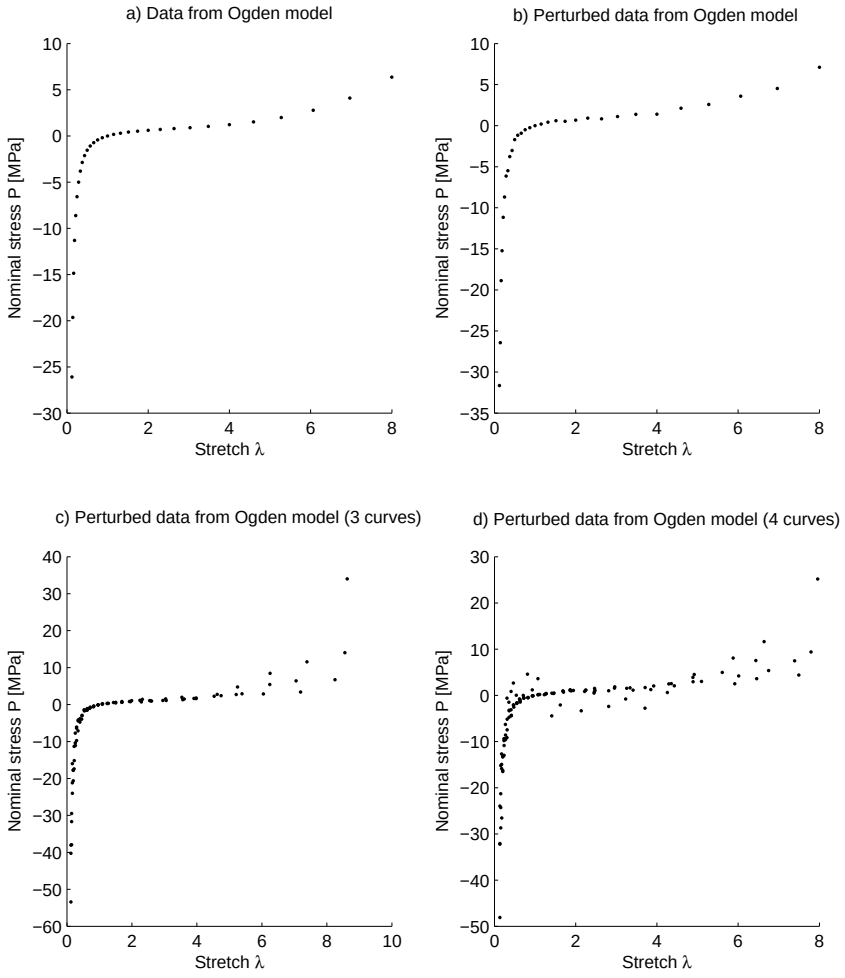

Figure 1: Computer-generated "experimental" data sets used in the examples. a) Exact data generated from Ogden's model. b) Data obtained using a small random perturbation in data obtained from Ogden's model, shown in (a). c) Three data sets obtained using perturbed Ogden parameters for each experimental point. d) Data obtained as in case (c), but with an additional curve with white noise.

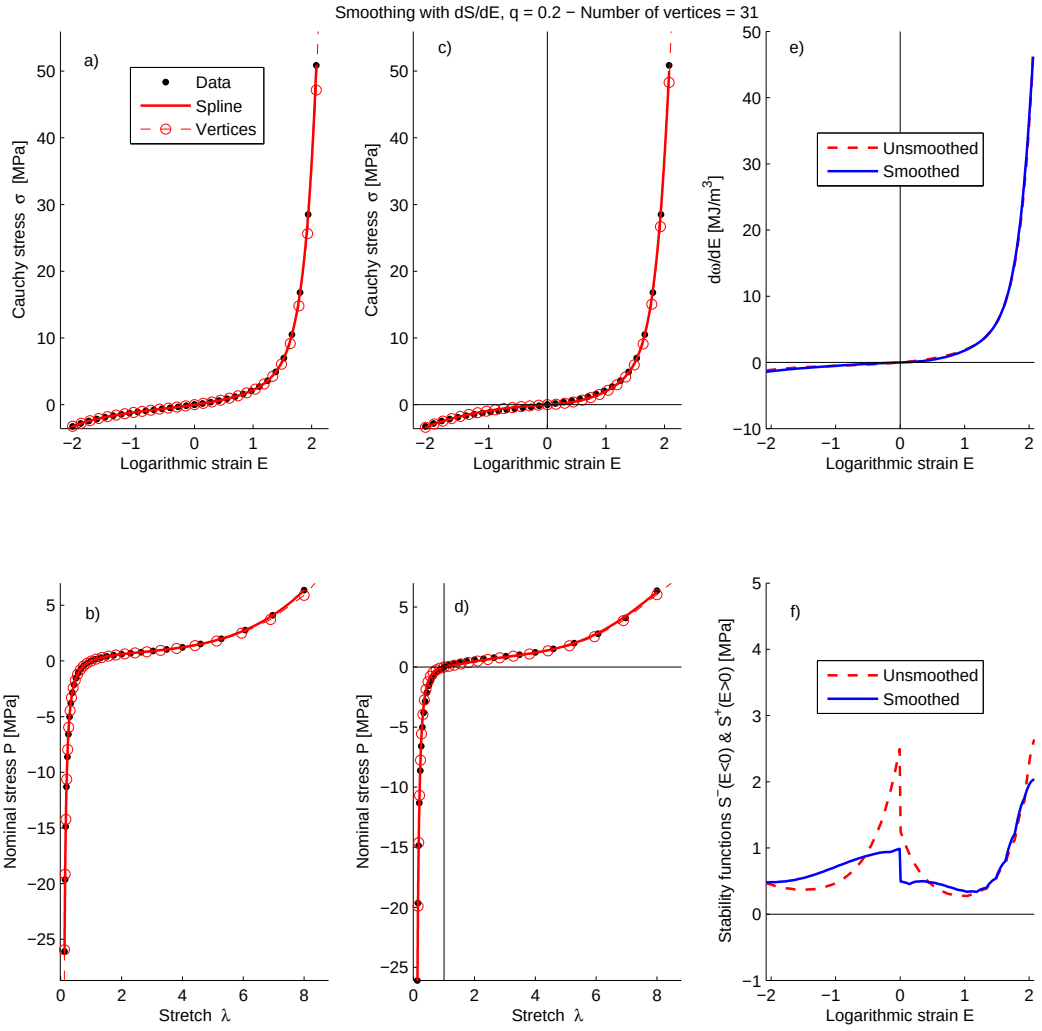

Figure 2: B-spline fit of data in Fig. 1a and related derivative of the stored energy $\omega'(E)$ computed using the WYPiWYG Sussman-Bathe procedure with inversion formula. Number of vertices of the B-spline: 31. Number of experimental data: 31. One additional experimental point is added at the origin. a) Predictions using unsmoothed B-splines in the $\sigma - E$ axes. b) Predictions using unsmoothed B-splines in the $P - \lambda$ axes. c) and d) Predictions using a smoothing with stability conditions and $q = 0.2$ (for ulterior comparisons). e) Derivative of the stored energies for smoothed and unsmoothed predictions. f) Stability conditions S^- and S^+. This figure shows that the proposed smoothing has little influence in the result if experimental data is already smooth.

origin, an additional data point is added at the origin and a large weight is assigned to this point. The layout of the figures for all examples below is similar. In Figure 2a, the unsmoothed predictions are shown in the $\sigma - E$ axes, whereas in Figure 2b the plot is shown in the $P - \lambda$ axes. The regression to experimental data is performed in the P axis. In Figures 2a and 2b, it is seen that B-splines are capable of capturing accurately the experimental data. In Figures 2c and 2d, the predictions have been obtained including a smoothing based on the selected stability conditions with $q = 0.2$. This smoothing value will be the most successful in the other cases. Figures 2c and 2d, included only for comparison purposes, show that the smoothing barely affects the predictions if experimental data are smooth and correspond to a stable material. Figure 2e shows the derivative of the computed stored energy term $\omega'(E)$ by the WYPiWYG procedure and Figure 2f shows the stability conditions. It is seen that both stored energy functions are very close to each other, that $\omega''(E) > 0$ in all the domain (see Figure 2c) and that in the tests performed $dP/d\lambda > 0$ (see Figure 2d). In Figure 3 we show the predictions using 11 vertices. It is seen that the results are almost unaffected by the number of vertices if a reasonable number of them is included.

Figure 4 shows the predictions for the experimental data in Figure 1b using 11 vertices. It is seen that the predictions, even without explicit smoothing, are smooth, accurate and stable (except at large compressions). Hence, B-splines with fewer vertices than data naturally produce some degree of smoothness. Figure 5 shows the predictions when 31 vertices are employed. Obviously more vertices allow for a more accurate description of experimental curves. However, in this case, periodic B-splines are not different than usual interpolating splines, showing important wiggles and an undesired interpolant scheme. In the numerical experiments, the behaviour of open B-splines has been better for this case, but give disappointing results for more complicated cases. Thus, in general, smoothing is needed.

As mentioned, the typical smoothing employed in the literature is the integral of the curvature, approximated either by $\sigma''(E)$ of by $P''(\lambda)$, depending on the chosen regression. Figures 5c and 5d show a slight smoothing using σ'' with $q = 0.0001$. It is shown that this procedure gives smooth predictions without sacrificing accuracy in a relevant manner. The associated computed WYPiWYG stored energy function derivative terms are shown in Figure 5e. The stored energy function derivative for the unsmoothed case presents also nonphysical wiggles and lacks convexity in many points. However, the smooth case does not present the wiggles and the energy term is convex in all the domain. The tensile and equibiaxial stability conditions are shown in Figure 5f. Again, the unsmoothed case is unstable, but the smoothed case is stable. The value of $q = 0.0001$ has been computed automatically so the result

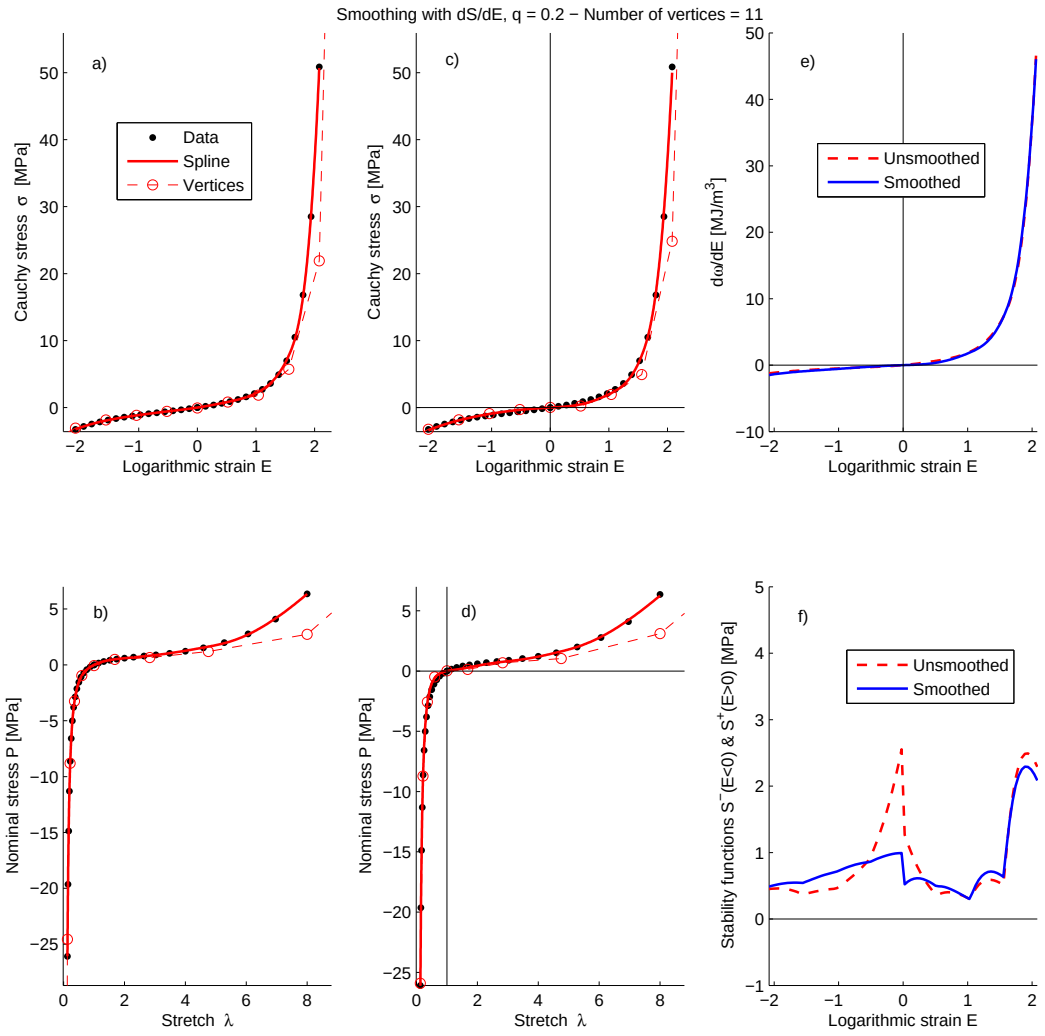

Figure 3: B-spline fit of data in Fig. 1a and related derivative of the stored energy $\omega'(E)$ computed using the WYPiWYG Sussman-Bathe procedure with inversion formula. Number of vertices of the B-spline: 11. Number of experimental data: 31. One additional experimental point is added at the origin. a) Predictions using unsmoothed B-splines in the $\sigma - E$ axes. b) Predictions using unsmoothed B-splines in the $P - \lambda$ axes. c) and d) Predictions using a smoothing with stability conditions and $q = 0.2$ (for ulterior comparisons). e) Derivative of the stored energies for smoothed and unsmoothed predictions. f) Stability conditions.

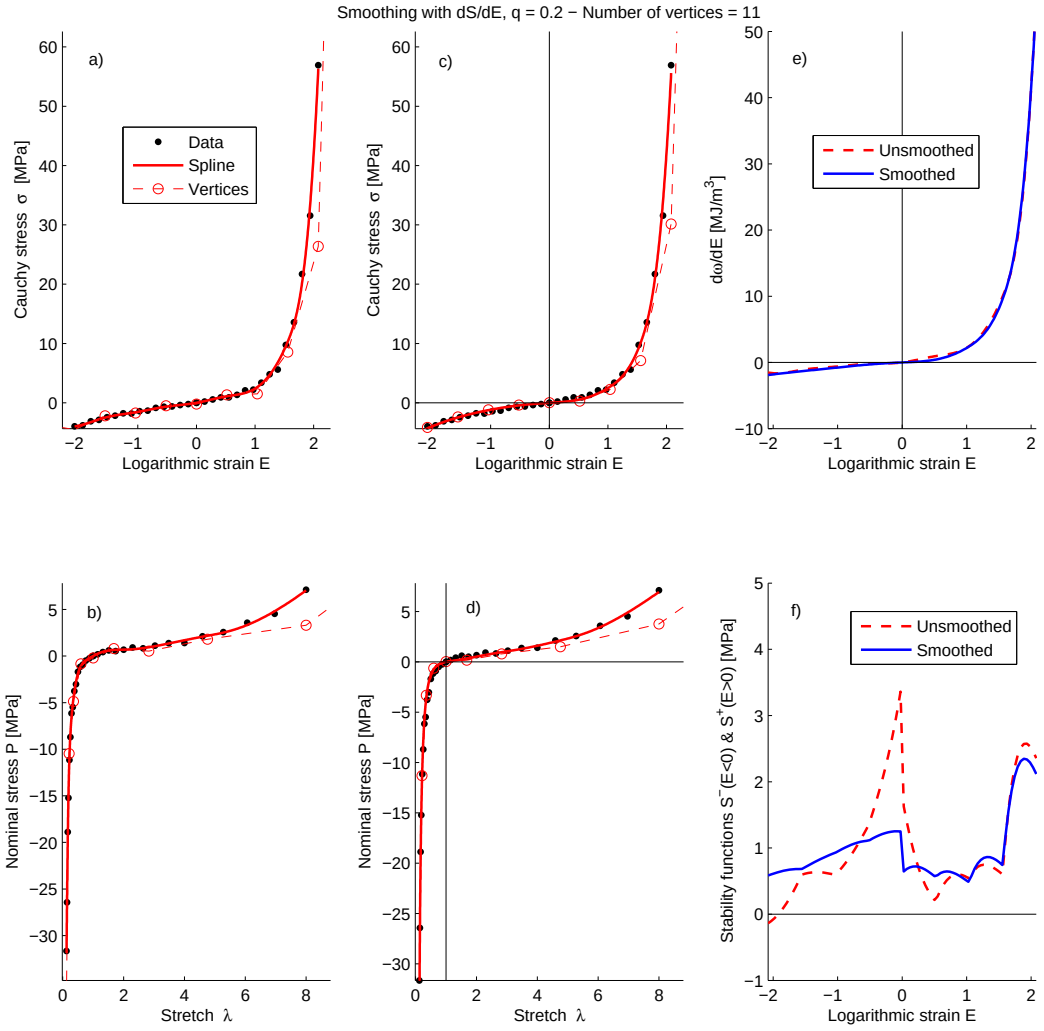

Figure 4: B-spline fit of data in Fig. 1b and related derivative of the stored energy $\omega'(E)$ computed using the WYPiWYG Sussman-Bathe procedure with inversion formula. Number of vertices of the B-spline: 11. Number of experimental data: 31. One additional experimental point is added at the origin. a) Predictions using unsmoothed B-splines in the $\sigma - E$ axes. b) Predictions using unsmoothed B-splines in the $P - \lambda$ axes. c) and d) Predictions using a smoothing with stability conditions and $q = 0.2$ (for ulterior comparisons). e) Derivative of the stored energies for smoothed and unsmoothed predictions. f) Stability conditions. This figure shows that using a small, but reasonable amount of vertices, is sufficient to capture the experimental curve to a high precision.

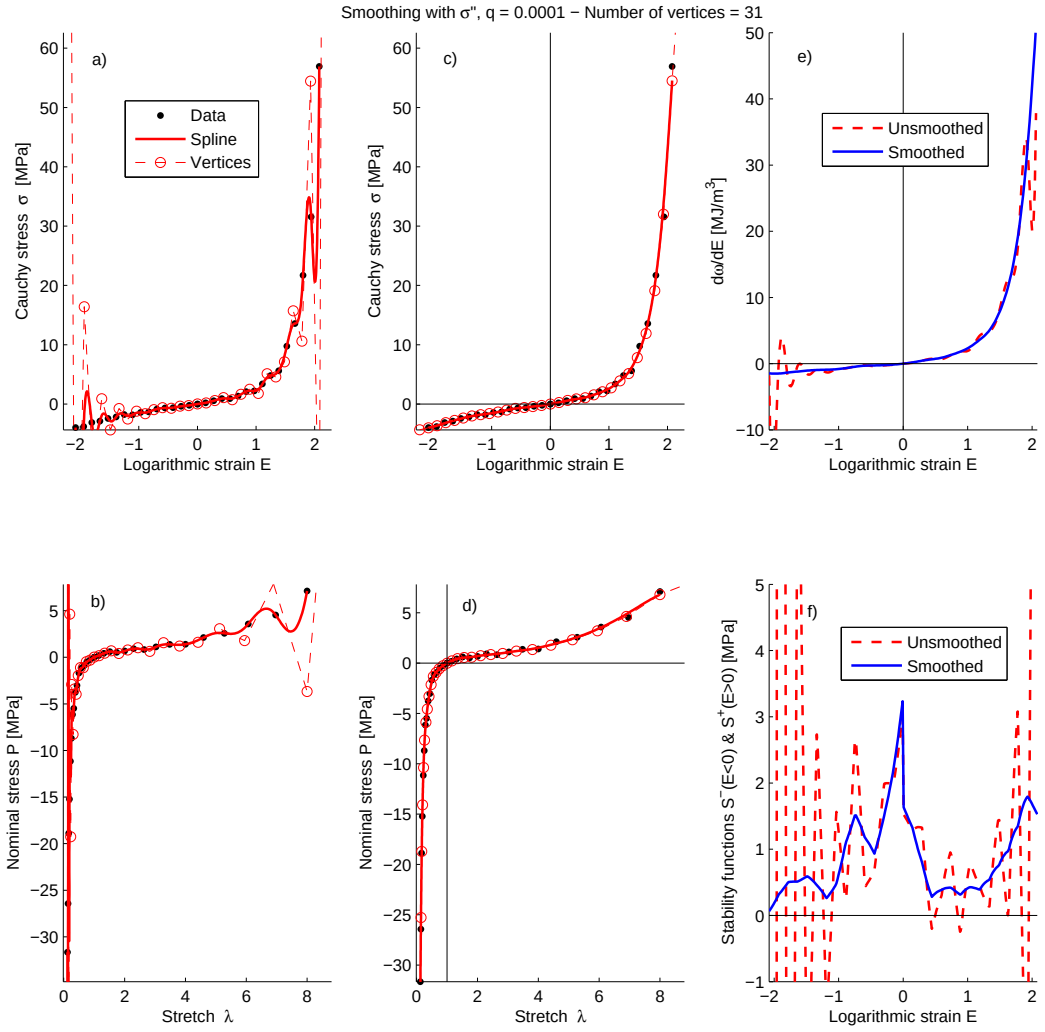

Figure 5: B-spline fit of data in Fig. 1b using 31 vertices; and related derivative of the stored energy $\omega'(E)$ computed using the WYPiWYG Sussman-Bathe procedure with inversion formula. a) and b) show respectively the $\sigma - E$ and $P - \lambda$ plots of the unsmoothed regression in the $\sigma - E$ axes. c) and d) shows the results using a smoothing function employing the curvature $\sigma''(E)$ and a small penalty parameter $q = 0.0001$. This figure shows that for small experimental errors, a smoothing using the curvature gives good results.

fulfills the stability conditions in all the computed domain. A similar result, not shown, is obtained if the penalty function is based on the stability conditions.

Figure 6 shows the predictions for the experimental data shown in Figure 1c, which consists in 93 pairs. In Figures 6a and 6b it is shown that even using less vertices than experimental data (hence not being interpolant), the result shows large wiggles, resulting in an unstable behavior. Figures 6c and 6d shows the predictions when performing a smoothing using the curvature of the $\sigma - E$ curve, and Figures 6e and 6f shows the predictions using a smoothing with the curvature of the $P - \lambda$ representation. The penalty employed is $q = 0.01$, which is a large number for the considered penalizing functions. These figures show that both cases (as well as their combinations not shown for brevity) produce unsatisfactory results because of the specific shapes of the stress-strain curves in hyperelastic materials, which naturally present large localized curvatures. Each smoothing procedure works only in the respective branch where the curvature is relatively small, but over-smoothes the other branch. Furthermore, although not shown, the corresponding stored energy functions are not stable.

Figure 7a and 7b shows the predictions for the experimental data shown in Figure 1c using 11 vertices and the penalty function which contains the stability conditions with $q = 0.2$. It is seen that in this case the predicted behavior is smooth and still following the tendency given by the experimental data. Figures 7c and 7d show the predictions if 51 vertices are used. No relevant differences are observed between both prediction sets, so 11 vertices are sufficient to capture the present material.

Finally, Figure 8 shows the predictions of the data in Figure 1d with smoothed B-splines, using the stability conditions in the penalty function with $q = 0.2$ and 51 vertices. It is seen that the resulting predictions are smooth and follow closely the tendencies given by the experimental data both in the tension and the compression branches. Furthermore, as it can be seen in Figure 8c the computed WYPiWYG stored energy term of the material is convex, and it can be observed in Figure 8d that the resulting material also fulfills the stability conditions for the tensile and equibiaxial tests.

In order to show the robustness of the procedure to variations in the number of vertices n and in the penalty parameter q, in Figure 9 we show different predictions obtained with $11, 31, 51$ and 91 vertices, and with q values of 0.05, 0.2 and 0.7. It can be observed that the differences are small in general. Only the case with $n = 11$, $q = 0.05$ results in a locally unstable behavior. In fact the value $q = 0.2$ has been computed automatically so that the case $n = 11$ fulfills the stability conditions. In Figure 9, it can also be observed that even though a smaller number of vertices ($n = 11$) yields smoother curves for unpenalized regression, when introducing

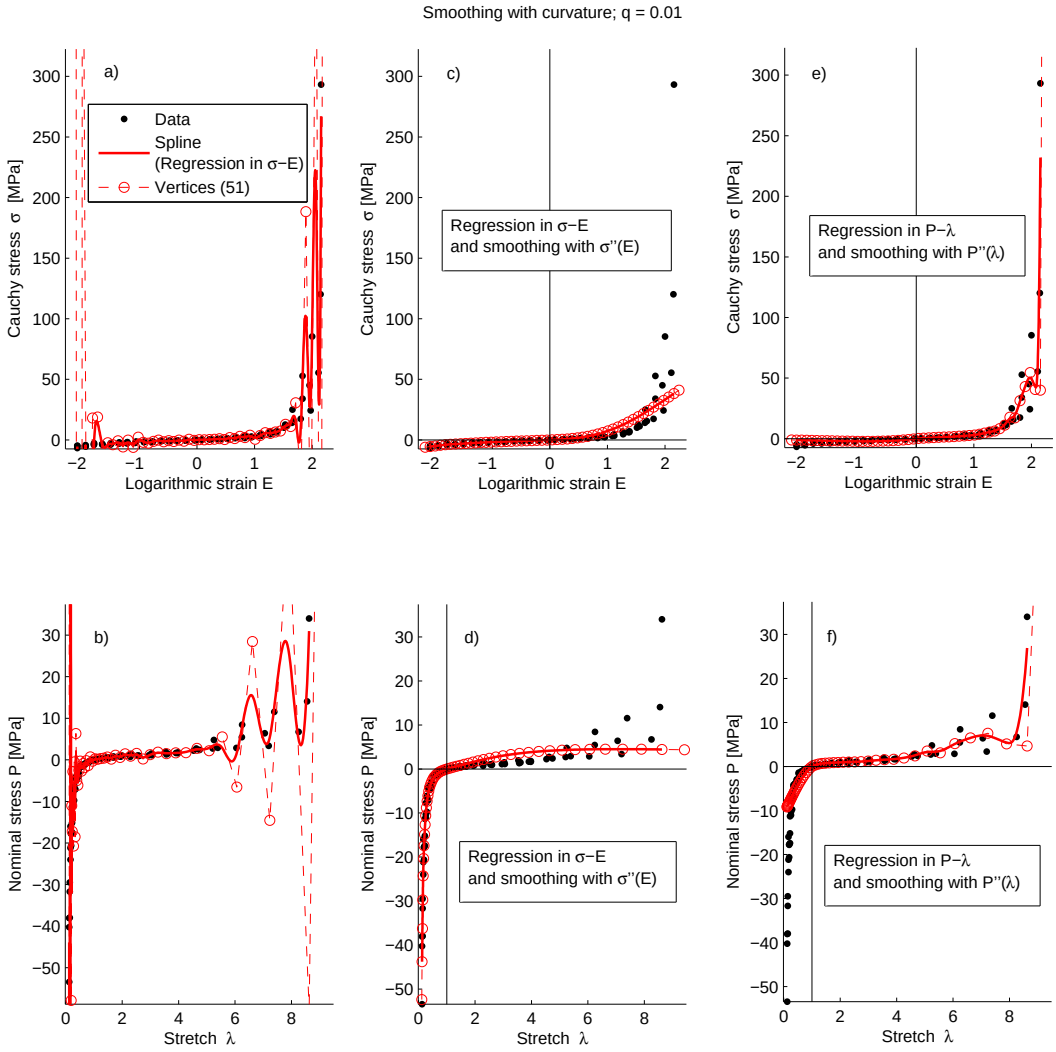

Figure 6: B-spline fits of the experimental data given in Figure 1c. a) and b) are respectively the $\sigma - E$ and $P - \lambda$ plots of the unsmoothed periodic B-spline with 51 vertices, with regression performed in the $\sigma - E$ domain (similar results are obtained for regression in the $P - \lambda$ domain). c) and d) are the smoothed predictions if smoothing is performed with curvature $\sigma''(E)$. e) and f) are the smoothed predictions if smoothing is performed with curvature $P''(\lambda)$; the same smoothing parameter $q = 0.01$ was used in both cases. This figure shows that needed curvature smoothing may eliminate the natural curvature of hyperelastic stress-strain functions; hence curvature smoothing is usefull only for light smoothings.

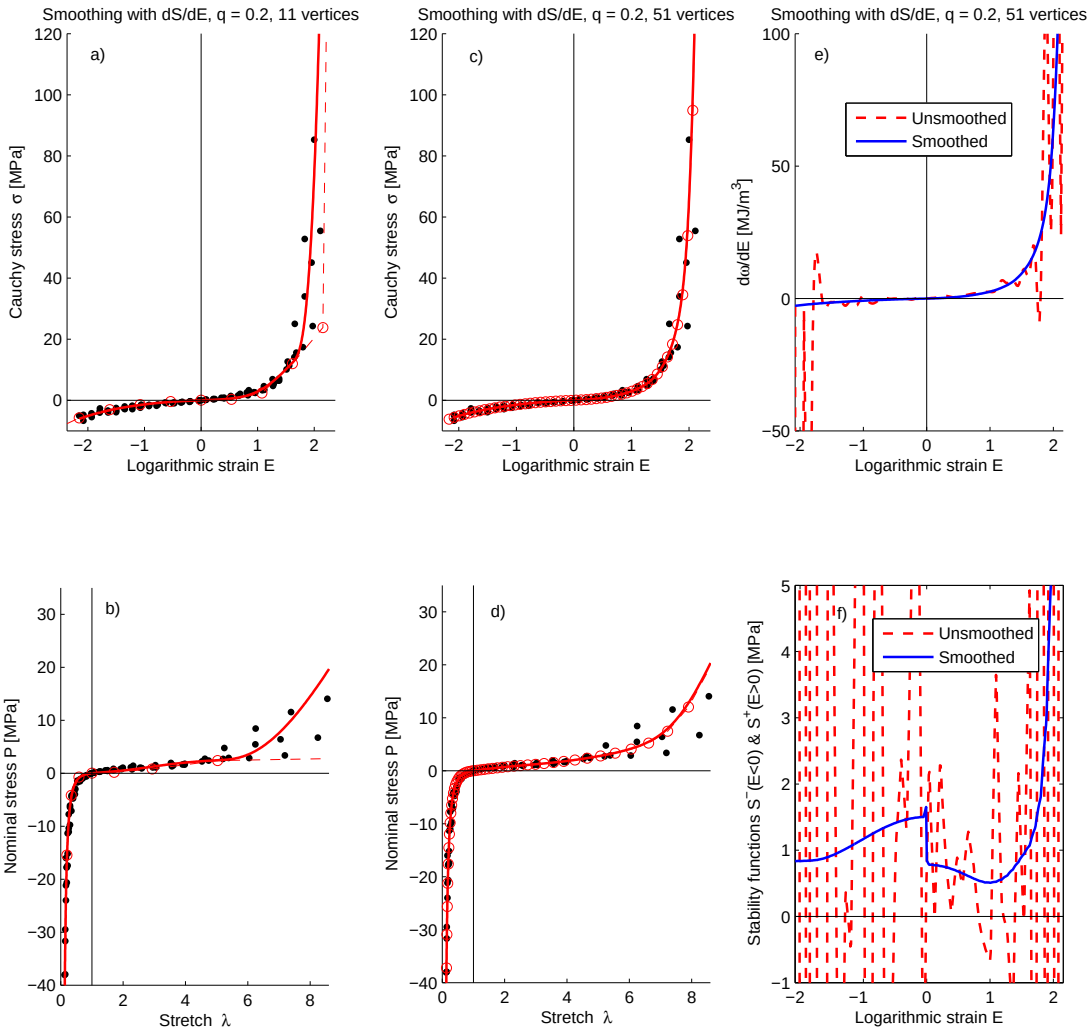

Figure 7: B-spline fits of the experimental data given in Figure 1c using stability conditions in the penalty function. a) and b) are the fits using 11 vertices. c) and d) are the fits using 51 vertices. e) Derivative of the stored energy term $\omega'(E)$ for the case of 51 vertices. f) Stability conditions. This figure shows that smoothing using stability conditions gives stable responses and smooth curves that keep the natural stress-strain curvature of the material data.

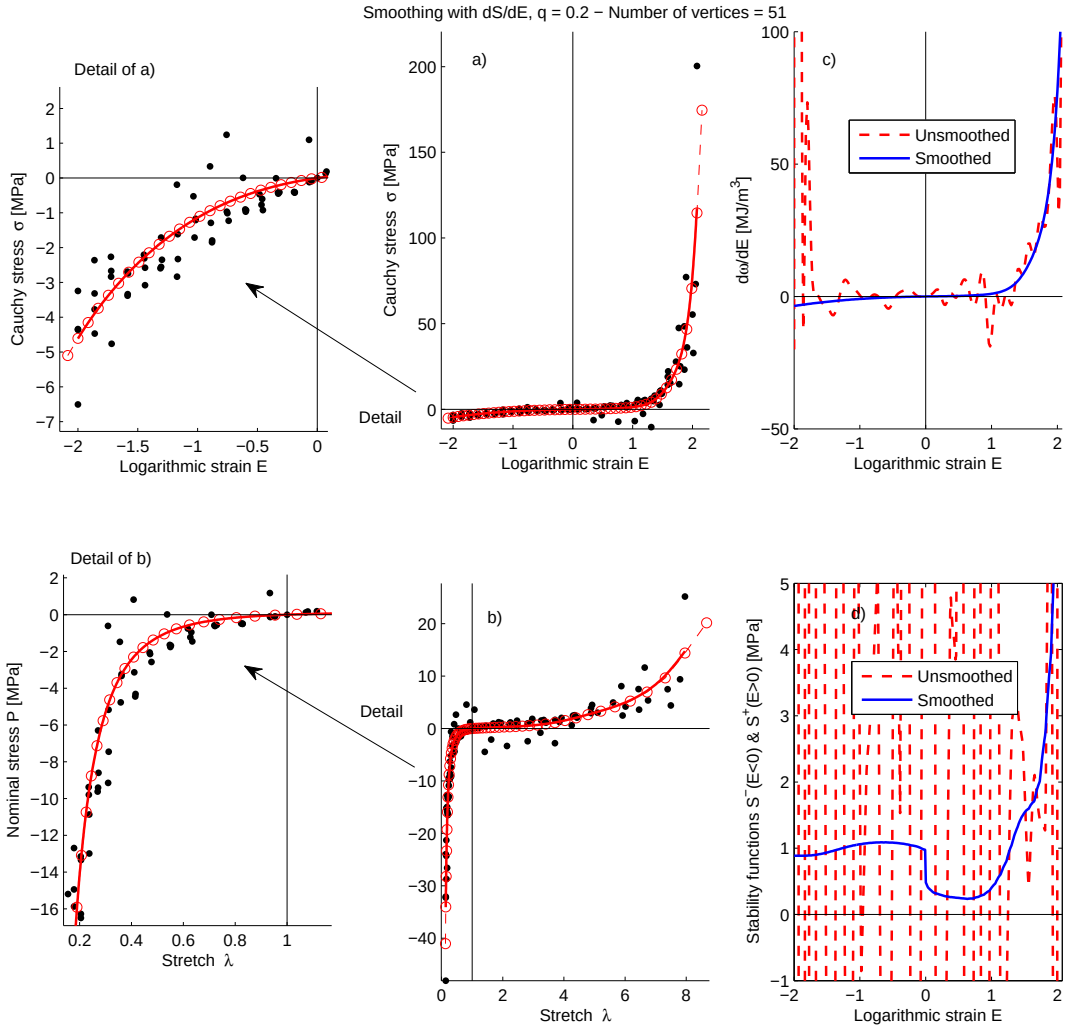

Figure 8: B-spline fits of the experimental data given in Figure 1d using 51 vertices and stability conditions in the penalty function. a) and b) are respectively the predictions in the $\sigma - E$ and $P - \lambda$ axes. Details of the compression branches are shown on the left. c) Stored energy derivative term $\omega'(E)$ for both the unsmooth and smooth cases. d) Stability conditions. This figure shows that the proposed method works well with very noisy data from different specimens.

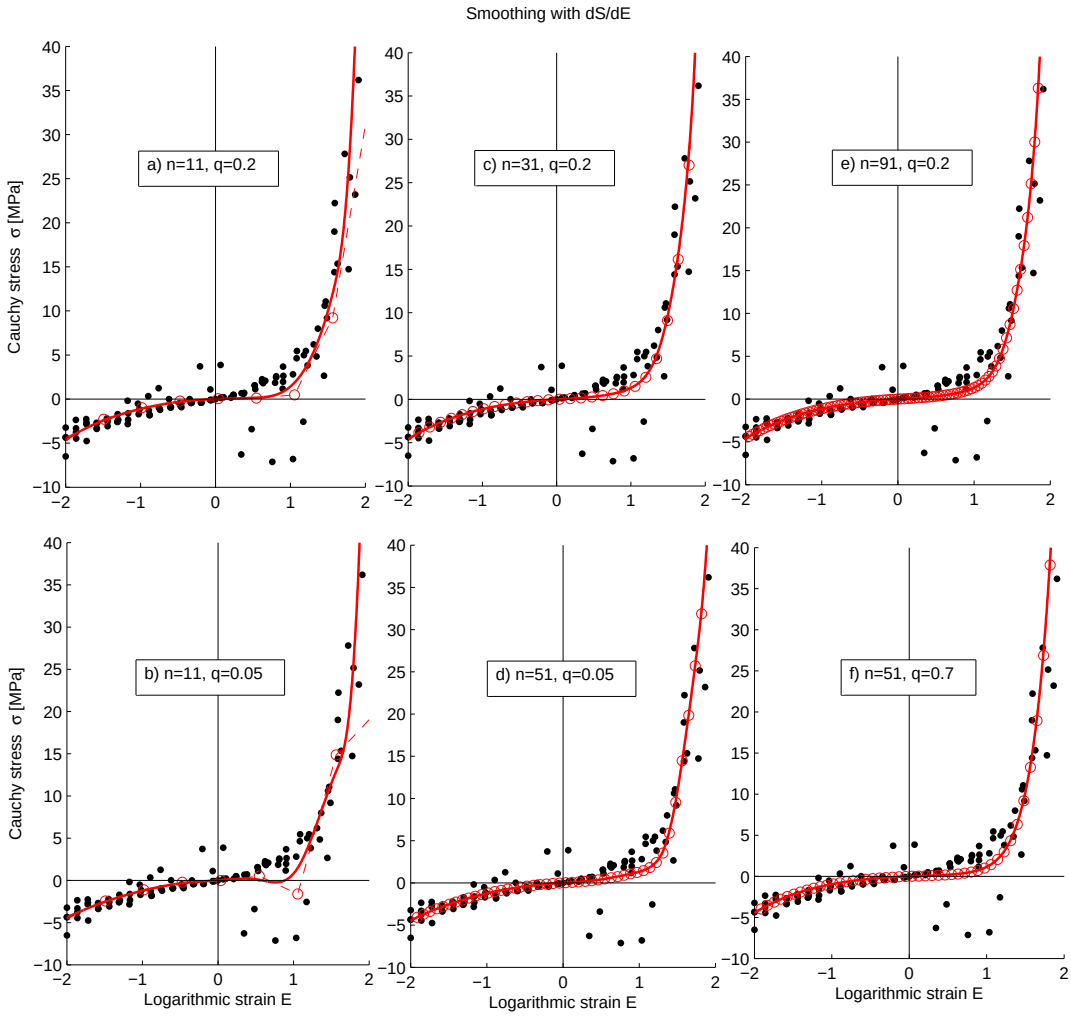

Figure 9: Different fits of the experimental data of Figure 1d employing a different number of vertices n and different penalty parameters q. The penalty function is written in terms of the stability conditions. This figure shows the robustness of the method by demonstrating the little sensitivity of the method to changes in the values of n and q.

penalizations, a reasonable amount of vertices produce better results and allow for lighter smoothing. An automatic selection of vertices may be easily implemented selecting a number, within some bounds, for which further refining produces changes smaller than a given tolerance.

9. Conclusions

In this paper we have presented a data reduction procedure for hyperelasticity based on smoothing regression B-splines. This data reduction procedure is convenient to obtain smooth and stable WYPiWYG stored energies in the presence of fuzzy experimental data or data from multiple specimens. The procedure can be used for other analytical models. We have shown that the typical smoothing based on curvatures is only useful for small experimental errors. Penalty smoothing functions based on stability conditions have proved to be robust in all cases, producing smooth and stable stored energy functions. The extension of these ideas to anisotropic cases is more involved and is ongoing research.

Of course, given a set of experimental data for a test, e.g. a tension-compression uniaxial test, the modeler may always guess a good smooth approximation of the observed behavior and just present data from that approximation to the model determination procedure. The associated strain energy can be numerically computed thanks to the inversion formula and spline interpolations. In that sense *splines are fine* [49]: the predicted behavior will be exactly the behavior prescribed by the modeler and smoothing of data is not too relevant. However, in order to avoid spurious local instabilities and make the procedure more automatic and less user-dependent, we have shown that *smoothing is soothing* [49].

Acknowledgements

Partial financial support for this work has been given by grant DPI2015-69801-R from the Dirección General de Proyectos de Investigación of the Ministerio de Economía y Competitividad of Spain.

A. Appendix: Open and periodic B-splines

Piecewise cubic splines are interpolant and controlled by the interpolated nodal values. On the contrary, B-splines are, in general, not interpolant and controlled by the vertices of a polygon. B-splines have been developed mainly in the CAD industry

from Bézier curves in order to numerically characterize and define smooth lines and surfaces [63]. The general form of the parametric B-splines is

$$\mathfrak{P}(t) = \sum_{i=1}^{n} N_i^{(k)}(t) B_i \quad \text{with } t_{\min} \leq t \leq t_{\max} \text{ and } 2 \leq k \leq n \tag{77}$$

where B_i are the position vector coordinates (either the coordinates x or y) of the n vertices of the control polygon, $\mathfrak{P}(t)$ is the result value (either the coordinates x or y at the parameter value t) and $N_i^{(k)}(t)$ are the corresponding normalized B-spline basis functions, having the partition of unity property. The matrix form of Eq. (77) is

$$\mathfrak{P}(t) = \boldsymbol{N}^{(k)}(t)\,\boldsymbol{B} = \left[N_1^{(k)}(t), ..., N_n^{(k)}(t)\right] \begin{bmatrix} B_1 \\ \vdots \\ B_n \end{bmatrix} \tag{78}$$

The B-spline basis functions are nowadays obtained through the Cox-de-Boor recursive formulae [63], [54], which basically implies a linear interpolation of the lower order functions:

$$N_i^{(k)}(t) = \frac{(t - t_i)}{(t_{i+k-1} - t_i)} N_i^{(k-1)}(t) + \frac{(t_{i+k} - t)}{(t_{i+k} - t_{i+1})} N_{i+1}^{(k-1)}(t) \tag{79}$$

with $k \geq 2$, and

$$N_i^{(1)}(t) = \begin{cases} 1 & \text{if } t_i \leq t < t_{i+1} \\ 0 & \text{otherwise} \end{cases}$$

where $\boldsymbol{t}$ is a vector of ordered *knots* such that $t_i \leq t_{i+1}$. The convention $0/0 = 0$ is taken (because we may encounter the case $t_i = t_{i+1}$). The B-spline derivatives are easily obtained through the chain rule, also in a recursive form.

Periodic B-splines may be defined by sequential knot vectors $t_i = i - 1$ with $i = 1, ..., k + n$, and normalized ξ parameters within each spline piece $0 \leq \xi \leq 1$. These B-splines may then be written in terms of the influencing vertices of each

spline as —note the abuse of notation when writing $\mathfrak{P}(t) = \mathfrak{P}(\xi)$

$$\mathfrak{P}_j(\xi) = \sum_{i=0}^{k-1} \bar{N}_{i+1}^{(k)}(\xi) B_{j+i} = \left[\bar{N}_1^{(k)}(\xi), ..., \bar{N}_k^{(k)}(\xi)\right] \begin{bmatrix} B_j \\ \vdots \\ B_{j+k-1} \end{bmatrix} \tag{80}$$

$$= \underset{\text{elem } j}{[0, ..., 0,} \underset{\bar{N}_1^{(k)}(\xi)}{} , ..., \underset{\text{elem } j+k}{\bar{N}_k^{(k)}(\bar{\xi})} , 0, ..., 0] \begin{bmatrix} B_1 \\ \vdots \\ B_j \\ \vdots \\ B_{j+k-1} \\ \vdots \\ B_n \end{bmatrix} \tag{81}$$

with the segment index taking the restricted useful values $1 \leq j \leq m$ with $m := n - k + 1$, see Figure 10. In this case the basis $\bar{N}_{i+1}^{(k)}(\xi)$ spread k intervals but are always the same and periodically repeated, hence the name, see Figure 10. Since periodic B-splines span $m \equiv n - k + 1$ segments and do not reach the initial and end vertices, additional $k - 2$ vertices may be attached to the spline or pseudovertices may be placed at given locations, see [63] for further details. For the case $k = 4$, the one used below, two additional vertices may be given at both ends of the spline; in Figure 10 we labeled them as "unused".

A.1. Relation between B-splines and piecewise cubic splines

Until now, we have used piecewise cubic splines as interpolation functions in WYPiWYG hyperelasticity. However, many other functions may be employed. The representation used by B-splines may have some advantages over that of classical splines; for example, imposing convexity on the multilinear hull, guarantees the convexity of the resulting curve (called Strong Convex Hull Property), and changing the position of a vertex, only modifies the curve locally.

Periodic B-splines, Eq. (80), may be written in a convenient matrix format which also yields computationally efficient procedures. Using normalized ξ parameters

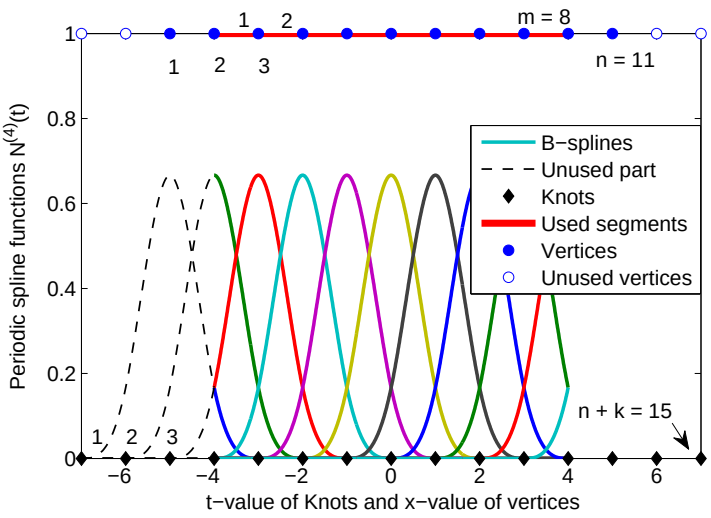

Figure 10: Base functions $N^{(4)}(t)$ of periodic splines (cubic B-splines, $k = 4$), knots ($n + k = 15$), $B-$vertices ($n = 11$ used with a unit value for plotting purposes), and segments ($m = n-k+1 = 8$).

within each spline piece $0 \leq \xi \leq 1$, for cubic B-splines we have

$$\begin{aligned} \mathfrak{P}_j(\xi) &= \left[\begin{array}{cccc} \xi^3 & \xi^2 & \xi & 1 \end{array}\right] \frac{1}{6} \left[\begin{array}{cccc} -1 & 3 & -3 & 1 \\ 3 & -6 & 3 & 0 \\ -3 & 0 & 3 & 0 \\ 1 & 4 & 1 & 0 \end{array}\right] \left[\begin{array}{c} B_j \\ B_{j+1} \\ B_{j+2} \\ B_{j+3} \end{array}\right] \\ &= \boldsymbol{\Xi}(\xi)\, \bar{\boldsymbol{N}} \boldsymbol{B}_j = \boldsymbol{N}_j(t(\xi))\, \boldsymbol{B} \end{aligned} \tag{82}$$

with $j = 1, ..., m$, where $m = n - 3$ and where $\boldsymbol{B}_j$ is the box of relevant vertices for each piece. On the other hand, piecewise cubic splines are defined by

$$\mathfrak{P}_j(\xi) = \left[\begin{array}{cccc} \xi^3 & \xi^2 & \xi & 1 \end{array}\right] \left[\begin{array}{c} d_j \\ c_j \\ b_j \\ a_j \end{array}\right] =: \boldsymbol{\Xi}(\xi)\, \boldsymbol{A}_j \tag{83}$$

so obviously the identification $\boldsymbol{A}_j = \bar{\boldsymbol{N}} \boldsymbol{B}_j$ together with equivalent ξ mappings (i.e. we will use $t = x$ as in piecewise cubic splines) bring an exact conversion from uniform periodic B-splines to equivalent uniform piecewise cubic splines. In Eq. (82) we take $j = 1$ for the first used vertex (the two vertices $j = 0$ and $j = -1$ are not

used and not included in n, see Figure 10). Recall also that $\boldsymbol{B}$ contains the vertices of the polygon defining the splines, but the splines do not pass through those points. Similar matrix expressions may be used for cubic splines, see [64], but in this case in terms of the interpolated points.

The periodic spline derivatives may also be obtained directly from the matrix form as

$$\begin{aligned}\mathfrak{P}_j'(\xi) &= \left[\begin{array}{cccc} 3\xi^2 & 2\xi & 1 & 0 \end{array}\right] \frac{1}{6} \left[\begin{array}{cccc} -1 & 3 & -3 & 1 \\ 3 & -6 & 3 & 0 \\ -3 & 0 & 3 & 0 \\ 1 & 4 & 1 & 0 \end{array}\right] \left[\begin{array}{c} B_j \\ B_{j+1} \\ B_{j+2} \\ B_{j+3} \end{array}\right] \\ &= \boldsymbol{\Xi}'(\xi)\, \bar{\boldsymbol{N}} \boldsymbol{B}_j \end{aligned} \tag{84}$$

and in a similar form $\mathfrak{P}_j''(\xi) = \boldsymbol{\Xi}''(\xi)\, \bar{\boldsymbol{N}} \boldsymbol{B}_j$ and $\mathfrak{P}_j'''(\xi) = \boldsymbol{\Xi}'''(\xi)\, \bar{\boldsymbol{N}} \boldsymbol{B}_j$. Note that in these equations the prima decoration implies derivative respect to the variable in parenthesis.

References

[1] M. Kojić, K.-J. Bathe, Studies of finite element procedures-Stress solution of a closed elastic strain path with stretching and shearing using the updated Lagrangian Jaumann formulation, Computers and Structures 26 (1-2) (1987) 175–179.

[2] K.-J. Bathe, Finite element procedures, 2nd Ed, Klaus-Jürgen Bathe, 2014.

[3] R. W. Ogden, Non-linear Elastic Deformations, Dover, New York, 1997.

[4] G. A. Holzapfel, Nonlinear Solid Mechanics, Vol. 24, Wiley Chichester, 2000.

[5] K. Volokh, Mechanics of Soft Materials, Springer, Singapore, 2006.

[6] P. Steinmann, M. Hossain, G. Possart, Hyperelastic models for rubber-like materials: consistent tangent operators and suitability for Treloars data, Archive of Applied Mechanics 82 (9) (2012) 1183–1217.

[7] T. Beda, An approach for hyperelastic model-building and parameters estimation a review of constitutive models, European Polymer Journal 50 (2014) 97–108.

[8] G. Marckmann, E. Verron, Comparison of hyperelastic models for rubber-like materials, Rubber Chemistry and Technology 79 (5) (2006) 835–858.

[9] V. Vahapoğlu, S. Karadeniz, Constitutive equations for isotropic rubber-like materials using phenomenological approach: A bibliography (1930–2003), Rubber Chemistry and Technology 79 (3) (2006) 489–499.

[10] J. M. Benítez, F. J. Montáns, The mechanical behavior of skin: Structures and models for the finite element analysis, Computers & Structures 190 (2017) 75–107.

[11] C. Miehe, Numerical computation of algorithmic (consistent) tangent moduli in large-strain computational inelasticity, Computer Methods in Applied Mechanics and Engineering 134 (3-4) (1996) 223–240.

[12] M. Tanaka, T. Sasagawa, R. Omote, M. Fujikawa, D. Balzani, J. Schröder, A highly accurate 1st-and 2nd-order differentiation scheme for hyperelastic material models based on hyper-dual numbers, Computer Methods in Applied Mechanics and Engineering 283 (2015) 22–45.

[13] J. Fike, J. Alonso, The development of hyper-dual numbers for exact second-derivative calculations, in: 49th AIAA Aerospace Sciences Meeting including the New Horizons Forum and Aerospace Exposition, 2011, p. 886.

[14] L. Infeld, et al., Quest, the Evolution of a Scientist, Doubleday, Doran & co., Inc., 1941.

[15] D. González, E. Cueto, F. Chinesta, Computational patient avatars for surgery planning, Annals of biomedical engineering 44 (1) (2016) 35–45.

[16] S. Niroomandi, I. Alfaro, D. Gonzalez, E. Cueto, F. Chinesta, Real-time simulation of surgery by reduced-order modeling and x-fem techniques, International journal for numerical methods in biomedical engineering 28 (5) (2012) 574–588.

[17] E. Cueto, F. Chinesta, Real time simulation for computational surgery: a review, Advanced Modeling and Simulation in Engineering Sciences 1 (1) (2014) 11.

[18] C. Zopf, M. Kaliske, Numerical characterisation of uncured elastomers by a neural network based approach, Computers & Structures 182 (2017) 504–525.

[19] J. E. Aronson, T.-P. Liang, E. Turban, Decision support systems and intelligent systems, Pearson Prentice-Hall, 2005.

[20] M. W. Craven, J. W. Shavlik, Using neural networks for data mining, Future Generation Computer Systems 13 (2-3) (1997) 211–229.

[21] C. Miehe, S. Göktepe, F. Lulei, A micro-macro approach to rubber-like materialsPart I: the non-affine micro-sphere model of rubber elasticity, Journal of the Mechanics and Physics of Solids 52 (11) (2004) 2617–2660.

[22] R. Ibañez, E. Abisset-Chavanne, J. V. Aguado, D. Gonzalez, E. Cueto, F. Chinesta, A manifold learning approach to data-driven computational elasticity and inelasticity, Archives of Computational Methods in Engineering (2017) 1–11doi:10.1007/s11831-016-9197-9.

[23] R. Ibañez, D. Borzacchiello, J. V. Aguado, E. Abisset-Chavanne, E. Cueto, P. Ladeveze, F. Chinesta, Data-driven non-linear elasticity: constitutive manifold construction and problem discretization, Computational Mechanics (2017) 1–14.

[24] T. Kirchdoerfer, M. Ortiz, Data-driven computational mechanics, Computer Methods in Applied Mechanics and Engineering 304 (2016) 81–101.

[25] T. Kirchdoerfer, M. Ortiz, Data driven computing with noisy material data sets, arXiv preprint arXiv:1702.01574.

[26] M. Latorre, F. J. Montáns, What-You-Prescribe-is-What-You-Get orthotropic hyperelasticity, Computational Mechanics 53 (6) (2014) 1279–1298.

[27] J. Crespo, M. Latorre, F. J. Montáns, WYPIWYG hyperelasticity for isotropic, compressible materials, Computational Mechanics 59 (1) (2017) 73–92.

[28] T. Sussman, K.-J. Bathe, A model of incompressible isotropic hyperelastic material behavior using spline interpolations of tension–compression test data, Communications in Numerical Methods in Engineering 25 (1) (2009) 53–63.

[29] E. Kearsley, L. Zapas, Some methods of measurement of an elastic strain-energy function of the Valanis-Landel type, Journal of Rheology 24 (4) (1980) 483–500.

[30] L. R. G. Treloar, The physics of rubber elasticity, Oxford University Press, Oxford, 1975.

[31] M. Latorre, F. J. Montáns, Extension of the Sussman–Bathe spline-based hyperelastic model to incompressible transversely isotropic materials, Computers & Structures 122 (2013) 13–26.

[32] M. Miñano, F. J. Montáns, WYPiWYG damage mechanics for soft materials: A data-driven approach, Archives of Computational Methods in Engineering (2017) 1–29.

[33] M. Latorre, F. J. Montáns, Strain-level dependent nonequilibrium anisotropic viscoelasticity: Application to the abdominal muscle, Journal of Biomechanical Engineering 139 (10) (2017) 101007.

[34] M. Latorre, X. Romero, F. J. Montáns, The relevance of transverse deformation effects in modeling soft biological tissues, International Journal of Solids and Structures 99 (2016) 57–70.

[35] J. Murphy, Evolution of anisotropy in soft tissue, in: Proceedings of the Royal Society A—Mathematical, Physical and Engineering Sciences, Vol. 470, The Royal Society, 2014, p. 20130548.

[36] E. De Rosa, M. Latorre, F. J. Montáns, Capturing anisotropic constitutive models with WYPiWYG hyperelasticity; and on consistency with the infinitesimal theory at all deformation levels, International Journal of Non-Linear Mechanics 96 (2017) 75–92.

[37] M. Miñano, J. Crespo, M. Latorre, F. J. Montáns, Advances in WYPIWYG constitutive modelling of soft materials, in: A. Zingoni (Ed.), Insights and Innovations in Structural Engineering, Mechanics and Computation: Proceedings of the Sixth International Conference on Structural Engineering, Mechanics and Computation, CRC Press, 2016, pp. 414–418.

[38] D. Robertson, D. Cook, Unrealistic statistics: how average constitutive coefficients can produce non-physical results, Journal of the Mechanical Behavior of Biomedical Materials 40 (2014) 234–239.

[39] D. D. Cook, D. J. Robertson, The generic modeling fallacy: Average biomechanical models often produce non-average results!, Journal of Biomechanics 49 (15) (2016) 3609–3615.

[40] M. Latorre, E. Peña, F. J. Montáns, Determination and finite element validation of the WYPIWYG strain energy of superficial fascia from experimental data, Annals of Biomedical Engineering 45 (3) (2017) 799–810.

[41] X. Romero, M. Latorre, F. J. Montáns, Determination of the WYPiWYG strain energy density of skin through finite element analysis of the experiments on circular specimens, Finite Elements in Analysis and Design 134 (2017) 1–15.

[42] M. C. Meyer, Constrained penalized splines, Canadian Journal of Statistics 40 (1) (2012) 190–206.

[43] B. W. Silverman, Some aspects of the spline smoothing approach to non-parametric regression curve fitting, Journal of the Royal Statistical Society. Series B (Methodological) (1985) 1–52.

[44] P. H. Eilers, B. D. Marx, Flexible smoothing with B-splines and penalties, Statistical science (1996) 89–102.

[45] E. Eisen, I. Agalliu, S. Thurston, B. Coull, H. Checkoway, Smoothing in occupational cohort studies: an illustration based on penalised splines, Occupational and Environmental Medicine 61 (10) (2004) 854–860.

[46] B. D. Marx, P. H. Eilers, Generalized linear regression on sampled signals and curves: a P-spline approach, Technometrics 41 (1) (1999) 1–13.

[47] L. M. Kocić, G. Milovanović, Shape preserving approximations by polynomials and splines, Computers & Mathematics with Applications 33 (11) (1997) 59–97.

[48] L. A. Piegl, W. Tiller, Least-squares B-spline curve approximation with arbitary end derivatives, Engineering with Computers 16 (2) (2000) 109–116.

[49] K. Steenland, Smoothing is soothing, and splines are fine, Occupational and Environmental Medicine 62 (2005) 141–142.

[50] E. Mammen, J. Marron, B. Turlach, M. Wand, et al., A general projection framework for constrained smoothing, Statistical Science 16 (3) (2001) 232–248.

[51] B. A. Turlach, Shape constrained smoothing using smoothing splines, Computational Statistics 20 (1) (2005) 81–104.

[52] B. J. McCartin, Theory of exponential splines, Journal of Approximation Theory 66 (1) (1991) 1–23.

[53] J. W. Schmidt, W. Hess, Quadratic and related exponential splines in shape preserving interpolation, Journal of Computational and Applied Mathematics 18 (3) (1987) 321–329.

[54] C. De Boor, A Practical Guide to Splines, Springer-Verlag, New York, 1978.

[55] P. Dierckx, Curve and Surface Fitting with Splines, Oxford University Press, Oxford, 1995.

[56] H. L. Weinert, Fast Compact Algorithms and Software for Spline Smoothing, Springer-Verlag, New York, 2013.

[57] H. Greiner, A survey on univariate data interpolation and approximation by splines of given shape, Mathematical and Computer Modelling 15 (10) (1991) 97–106.

[58] M. Latorre, E. De Rosa, F. J. Montáns, Understanding the need of the compression branch to characterize hyperelastic materials, International Journal of Non-Linear Mechanics 89 (2017) 14–24.

[59] R. Ogden, G. Saccomandi, I. Sgura, Fitting hyperelastic models to experimental data, Computational Mechanics 34 (6) (2004) 484–502.

[60] S. Hartmann, P. Neff, Polyconvexity of generalized polynomial-type hyperelastic strain energy functions for near-incompressibility, International Journal of Solids and Structures 40 (11) (2003) 2767–2791.

[61] J. E. Marsden, T. J. Hughes, Mathematical Foundations of Elasticity, Courier Corporation, 1994.

[62] C. Truesdell, W. Noll, The Non-linear Field Theories of Mechanics, Springer, Berlin, 2004.

[63] D. F. Rogers, An introduction to NURBS: with historical perspective, Elsevier, 2000.

[64] M. Latorre, F. J. Montáns, WYPiWYG hyperelasticity without inversion formula: Application to passive ventricular myocardium, Computers & Structures 185 (2017) 47–58.